INFORMATION TO USERS

This manuscript has been reproduced from the microfilm master. UMI films the text directly from the original or copy submitted. Thus, some thesis and dissertation copies are in typewriter face, while others may be from any type of computer printer.

The quality of this reproduction is dependent upon the quality of the copy submitted. Broken or indistinct print, colored or poor quality illustrations and photographs, print bleedthrough, substandard margins, and improper alignment can adversely affect reproduction.

In the unlikely event that the author did not send UMI a complete manuscript and there are missing pages, these will be noted. Also, if unauthorized copyright material had to be removed, a note will indicate the deletion.

Oversize materials (e.g., maps, drawings, charts) are reproduced by sectioning the original, beginning at the upper left-hand corner and continuing from left to right in equal sections with small overlaps.

Photographs included in the original manuscript have been reproduced xerographically in this copy. Higher quality 6" x 9" black and white photographic prints are available for any photographs or illustrations appearing in this copy for an additional charge. Contact UMI directly to order.

Bell & Howell Information and Learning
300 North Zeeb Road, Ann Arbor, MI 48106-1346 USA
800-521-0600

UMI®

Downloaded from SHAREOK. Persistent Handle URL: https://hdl.handle.net/11244/295

NOTE TO USERS

This reproduction is the best copy available.

UMI®

UNIVERSITY OF OKLAHOMA

GRADUATE COLLEGE

PERFORMANCE EVALUATION OF CDMA SYSTEMS

A Dissertation

SUBMITTED TO THE GRADUATE FACULTY

in partial fulfillment of the requirements for the

degree of

Doctor of Philosophy

By

HELEN JUN XING
Norman, Oklahoma
2001

UMI Number: 3004888



UMI Microform 3004888

Copyright 2001 by Bell & Howell Information and Learning Company.
All rights reserved. This microform edition is protected against unauthorized copying under Title 17, United States Code.

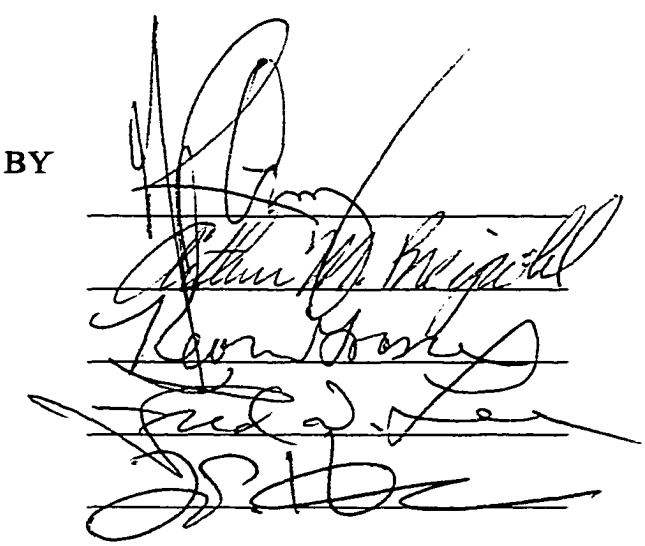
Bell & Howell Information and Learning Company
300 North Zeeb Road
P.O. Box 1346
Ann Arbor, MI 48106-1346

© Copyright by HELEN JUN XING 2001
All Rights Reserved.

PERFORMANCE EVALUATION OF CDMA SYSTEMS

A Dissertation APPROVED FOR THE
SCHOOL OF ELECTRICAL AND COMPUTER ENGINEERING

BY



ACKNOWLEDGEMENTS

I gratefully acknowledge Dr. J. R. Cruz, my chief advisor, for his guidance, encouragement and support throughout the research phase. Without him, I would not have been able to complete the projects and this thesis. It is a great pleasure and honor to work with him. I also wish to express my sincere appreciation to Dr. Kevin A. Grasse for discussions in combined probability density function of variables. My sincere appreciation is extended to Dr. Art M. Breipohl for his constructive comments and excellent lectures in random signals. Thanks are also due to Dr. Fred N. Lee and Dr. Joseph P. Havlicek for their advice and assistance. I am blessed to have such a wonderful committee.

I am also appreciative of Yiping Wang, a former Ph. D. student of Dr. Cruz, for his precious help on the cooperative projects with Nortel Networks. My special thanks go to Dr. David. W. Paranchych in Nortel Networks for his contribution with the simulations of the turbo codes and Richard M. Todd, one of my lab mates, for the design of the LDPC codes.

I am thankful to my other lab mates in the Communications Signal Processing Laboratory for their kind help. I especially enjoy the discussions and collaborations with John W. Wustenberg, Hongxin Song, Shuqing Liu, Cheng Zhong and Rodney C. Keele.

I would like to express my special gratitude to my parents, Shuyin Xing and Zhihua Liu, for their support, love and confidence. Without their help, this thesis would have been impossible.

Last, but not least, I would like to thank my dearest husband Jun, whose understanding, support and encouragement have been incredible.

This dissertation is dedicated to my beloved eight months old baby son

Michael.

TABLE OF CONTENTS

Acknowledgements ..... **iv**

Table of Contents ..... **vii**

List of Tables ..... **ix**

List of Figures ..... **x**

Abstract ..... **xii**

Chapter 1. Introduction **1**

1.1. What is CDMA 1

1.2. Development of CDMA 2

1.3. Capacity of CDMA Cellular Systems 3

1.4. Digital Beamforming for CDMA Cellular Systems 5

1.5. Coding Techniques for CDMA Cellular Systems 6

1.6. Overview 7

Chapter 2. Antenna Performance Comparisons for IS-95 CDMA Systems ... 9

2.1. Introduction 9

2.2. Simulation Procedure 10

2.2.1. IS-95 System Simulation 10

2.2.1.1. Transmitter Description 10

2.2.1.2. Channel Modeling 14

2.2.1.3. Receiver Description 17

2.2.1.4. Power Control Techniques 21

2.2.1.5. Soft Output Decision Decoding (SOVA) 23

2.2.2. Adaptive Antenna Arrays 24

2.2.3. Switching Beam Antennas 28

2.3. Simulation Assumptions and Results 29

2.4. Conlusions 40

Chapter 3. Low-Density Parity-Check Codes for IS-2000 CDMA Systems.. 42

3.1. Introduction 42

3.2. System Modeling 43

3.3. LDPC Code Design 48

3.4. Convolutional and Turbo Code Specifications 51

3.5. Simulation 51

3.6. Decoding Complexity and Memory Requirement 57

3.7. Theoretical Noisy Channel Estimates 59

3.8. Conclusions 63

Chapter 4. Interference Analysis of CDMA Systems 65

4.1. Introduction 65

4.2. Analytical Model 68

4.3. Extended Combined PDF Approach 73

4.4. Shadowing Environment 75

4.4.1. Pure Fading 75

4.4.2. Viterbi's Log-normal Shadowing Model 77

4.4.3. Mawira's Shadowing Model 80

4.5. Sectorized Antennas in a Multicell Environment 82

4.6. Conclusions 86

Chapter 5. Conclusions 88

References 91

LIST OF TABLES

TABLE 2.1 QPSK SIGNAL MAPPING 14

TABLE 2.2 SETTING PARAMETERS FOR THE VALIDATION 30

TABLE 2.3 REQUIRED E_b/N_o AT A FIXED FER WITH NO FADING 31

TABLE 2.4 REQUIRED E_b/N_o AT A FIXED FER WITH ONE FADING PATH 31

TABLE 2.5 INITIAL CONDITIONS FOR THE SIMULATION SCENARIO 32

TABLE 2.6 REQUIRED INPUT SIR FOR FOUR USERS AND 10% FER 33

TABLE 2.7 INPUT SIR FOR TEN USERS AND 10% FER 35

TABLE 2.8 INPUT SIR FOR TWENTY USERS AND 10% FER 37

TABLE 2.9 REQUIRED INPUT SIR FOR THIRTY USERS AND 1% FER 38

TABLE 3.1 INTERLEAVER PARAMETERS 45

TABLE 3.2 SIMULATION PARAMETERS 53

TABLE 3.3 TRAFFIC POWER ALLOCATIONS FOR IS-2000 FORWARD LINK INCORPORATING LDPC CODING AND CONVOLUTIONAL CODING TECHNIQUES 55

TABLE 3.4 COMPARISON OF COMPLEXITY OF TURBO AND LDPC DECODING ... 57

TABLE 3.5 COMPARISON OF COMPLEXITY OF TURBO AND LDPC DECODING ... 58

LIST OF FIGURES

Fig. 1.1. A basic digital beamforming system. 5

Fig. 2.1. Reverse CDMA channel structure 10

Fig. 2.2. Impulse response of baseband filter 13

Fig. 2.3. Fast fading waveforms for speeds of 10 and 30 km/hr within one second period 15

Fig. 2.4. Autocorrelation functions for both simulated and theoretical Rayleigh waveforms. 16

Fig. 2.5. Imaginary part versus real part of autocorrelation functions of simulated Rayleigh waveforms 17

Fig. 2.6. Schematic diagram of non-coherent detection procedure 20

Fig. 2.7. Four element uniform linear array 25

Fig. 2.8. The convergence of the RLS adaptive array with fixed angle of arrival for the desired user 27

Fig. 2.9. Array beam pattern using RLS for four users with angles of arrival 0.0, -1.0, -0.5, 0.5 rads 28

Fig. 2.10. Array beam pattern with 30° beamwidth (HPBW) 29

Fig. 2.11. Comparison between adaptive arrays and fixed multibeam for four users and 10% FER 34

Fig. 2.12. Beampattern comparisons between adaptive arrays and fixed multibeam for four users and 10% FER 34

Fig. 2.13. Comparison between adaptive arrays and fixed multibeam for ten users and 10% FER 36

Fig. 2.14. Beampattern comparisons between adaptive arrays and fixed multibeam for ten users and 10% FER 36

Fig. 2.15. Comparison between adaptive arrays and fixed multibeam for twenty users and 10% FER 37

Fig. 2.16. Comparison between adaptive arrays and fixed multibeam for thirty users and 1% FER 39

Fig. 2.17. Beampattern comparisons between adaptive arrays and fixed multibeam for thirty users and 1% FER 39

Fig. 3.1. IS-2000 forward link 43

Fig. 3.2. Coding gain of LDPC over convolutional codes for AWGN channels 52

Fig. 3.3. Average transmitted power gain of LDPC over convolutional coding for the IS-2000 forward link 56

Fig. 3.4. Average transmitted power gain of turbo over convolutional coding for the IS-2000 forward link 56

Fig. 4.1. Hexagonal cell configuration 69

Fig. 4.2. Performance of 19-cell and 7-cell configuration at location (0.5, 0.5) for the forward link with different number of users 76

Fig. 4.3. Performance of a 7-cell configuration at location (0.5, 0.5) for the forward link with different number of users and b as a parameter 79

Fig. 4.4. Performance of 7-cell configuration incorporating Mawira's model at location (0.5, 0.5) for the forward link with different number of users 82

Fig. 4.5. Interfering sectors in a sectorized multicell environment 83

Fig. 4.6. Performance of sectorization of pure fading with finite front-to-back ratios 84

Fig. 4.7. Performance of sectorization of the system incorporating Viterbi's shadowing model with finite front-to-back ratios and $b^2 = 0.5$ 85

Fig. 4.8. Performance of sectorization of the system incorporating Mawira's shadowing model with finite front-to-back ratios 85

ABSTRACT

The performance of cellular CDMA systems is evaluated using both link level computer simulations and multicell numerical analysis methods. As two of the most commonly used techniques for performance enhancement of CDMA systems, beamforming and coding techniques are investigated.

As far as antenna systems are concerned, this dissertation compares the performance between adaptive antenna arrays and fixed multibeam techniques for the reverse link of IS-95 systems. It is found that adaptive beamforming performs best when the number of interferers is less than the number of antenna elements. However, when the number of interferers is large, fixed multibeam techniques, which can be more easily implemented in the practical world, outperform adaptive antenna arrays when the speeds of vehicles are higher.

Also, various coding techniques are compared for the forward link of IS-2000 systems in this dissertation. The possible application of low-density parity-check (LDPC) coding in CDMA systems is investigated. Its performance is compared with convolutional and turbo coding. Both LDPC and turbo coding outperform convolutional coding when the data rates are high. However, randomly generated LDPC codes cannot achieve as much gain over convolutional codes as turbo codes. Although LDPC codes require much less decoding complexity, they have larger memory requirements.

Performance evaluation in terms of bit error rate (BER) for a multicell environment is also done analytically and numerically in the latter part of this dissertation. The multiple access interfering signals coming upon the desired vehicle comprise of path loss, correlated log-normal shadowing and Rayleigh fast fading. With the help of the efficient combined probability density function (PDF) method, the BER expressions incorporating Viterbi's and Mawira's shadowing models and sectorized antennas with finite front-to-back ratios are derived and numerically evaluated.

Chapter 1

Introduction

1.1 What is CDMA ?

CDMA is the acronym for code-division multiple-access communication. CDMA is one of the spread spectrum techniques, which uses a much wider transmission bandwidth compared to the data rates of the users. Because the signal is spread over a very wide bandwidth, interference from other users within that bandwidth is small. This allows multiple users to share the radio channel simultaneously. CDMA systems can be classified as frequency-hopped CDMA (FH/CDMA) or direct-sequence CDMA (DS/CDMA) systems [1]. In an FH/CDMA system, the transmitter changes its carrier frequency at regular intervals according to a hopping pattern. In a DS/CDMA system, the transmitter phase-shift-keys its carrier with a very high rate pseudo-noise (PN) sequence. Code division means that a CDMA system allows several transmitters to share the available bandwidth by using different PN codes.

1.2 Development of CDMA

Spread spectrum techniques were first used in military applications. They found their first widespread commercial use in Equatorial Communications Company's C-band receive-only small satellite earth stations [2]. After Equatorial introduced its first micro earth-station product in 1981, it had sold over 10,000 such items by 1984. In 1985, the Federal Communications Commission (FCC) encouraged experimentation with spread spectrum communications. In December 1991, QUALCOMM presented the results of a CDMA system field trials. Written based on the QUALCOMM CDMA system, Interim Standard 95 (IS-95) was adopted by the Telecommunications Industry Association (TIA) in July 1993. Since then, CDMA has gained widespread international attention in wireless communications. It has been accepted as an upgrade to increase dramatically the system capacity and service quality. Two developments have resulted in CDMA's commercial applications. One was the availability of very low cost, high density digital integrated circuits. That made the mobile stations quite small and cheap. The other is the power control in the CDMA systems which can regulate transmitter's power to the lowest level and at the same time adequate signal quality is guaranteed. Since the bandwidth of IS-95 is relatively narrow (1.25 MHz), the IS-95 system is often called a narrowband CDMA. A revision of the standard (IS-95 A) was voted on and accepted in 1995 [3]. It is designed to be compatible with the existing U.S. analog cellular system frequency band, so it was proposed for dual mode operation. The reverse link of IS-95 system operates

in the 824-849 MHz band, while the forward link operates in the 869-894 MHz band. The maximum user data rate which IS-95 system supports is 9.6 kb/s.

The first generation of cellular technology was analog. The second generation of wireless was digital. The current digital cellular systems, like CDMA, GSM (Global System for Mobile Communications) and TDMA (Time Division Multiple Access), are not compatible with each other [2]. In order to consolidate these standards, the concept of 3rd generation (3G) communication systems was introduced by the International Telecommunications Union (ITU) in 1992. The ballot version of IS-2000 CDMA systems [4] proposed in 1999 is one example of a 3G communication system. Because the data rates for 3G CDMA systems are relatively high (as high as 2Mbit/sec) and allow more users to simultaneously access the system, they are usually called wideband CDMA systems. The significant concept distinguishing it from narrowband CDMA is the introduction of intercell asynchronous operation and pilot channels for each data channel both for the forward link and the reverse link, which enables the use of adaptive antenna arrays for further interference suppression [5].

1.3 Capacity of CDMA Cellular Systems

Cellular CDMA systems are limited in performance and capacity by two major impairments [6]. The first is the fading of the signal. Fading is artificially separated into two parts: long-term fading (which is also called slow fading) and

short-term fading (which is also called fast fading). Long-term fading is characterized as path loss and shadowing, which are mainly caused by the distance from the base station to the mobile unit and natural or man-made environment. Because this kind of fading is changing very slowly, it can be usually compensated by power control techniques. Power control means to regulate the transmitted power to equalize the average signal powers of all users received at a base station or received at the mobile users. However, short-term fading, which is caused by the accumulation of multiple paths of the transmitted signal at the receiver [7], can not be tracked by power control techniques. Usually, if the vehicle speed is higher, both the amplitude and the phases of the signal change relatively faster.

Another impairment for cellular CDMA systems is co-channel interference. Multiple users in multiple cells use the same radio frequency. Each user has its specific code to distinguish itself from other users. Since these codes cannot be exactly orthogonal to each other, as the number of simultaneous users in surrounding cells increases, the performance of the tagged mobile user will become poorer. The capacity of CDMA systems is strongly limited by multiple access interference from multiple cells. However, using several combined techniques including digital beamforming and coding, the maximum number of users which CDMA systems can support can be increased.

1.4 Digital Beamforming for CDMA Cellular Systems

Digital beamforming is one way to improve the capacity of CDMA cellular systems by exploiting space diversity [8]. In the wireless communications industry, it has attracted a great deal of attention and is being regarded as a core system component for future-generation networks. Digital beamforming combines antenna technologies and digital signal processing [9]. Fig. 1.1 is a basic digital beamforming system. After passing through the transceivers, the amplitudes and phases of the signals received at each element of the antenna arrays are obtained in digital form. The beamforming is carried out by adjusting these amplitudes and phases so that when they are added together, they form a new desired beam.

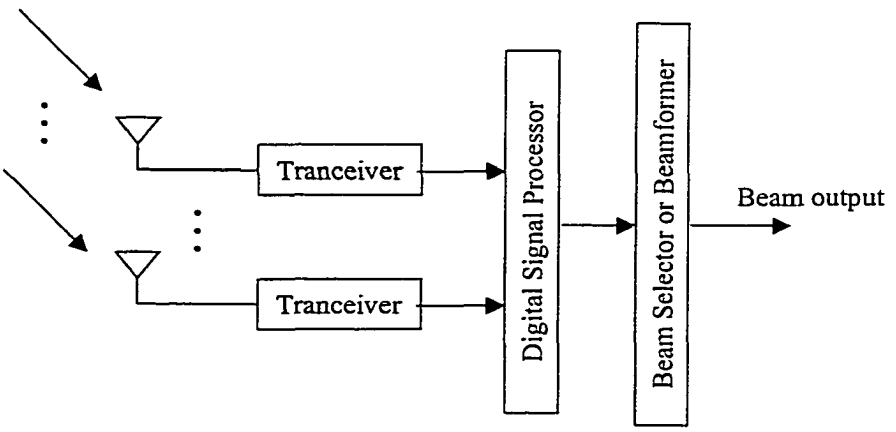


Fig. 1.1. A basic digital beamforming system.

1.5 Coding Techniques for CDMA Cellular Systems

Error control coding is another way of achieving reliable data transmission and improving the capacity of CDMA cellular systems. There are two different types of commonly used codes today: block codes and convolutional codes [10]. It is known that error-correction codes can improve communication performance relative to uncoded transmission, but no practical error correction coding system exists that can exceed the theoretical performance limit given by Shannon's law. In other words, Shannon proved that for any channel there exist families of codes that achieve arbitrarily small probability of error at any communication rate up to the maximum possible information transfer rate through a channel (subject to specified constraints), which is also called the capacity of a channel.

In 1962 Gallager introduced low-density parity-check binary codes [11]. The parity check matrix for this kind of code is very sparse (the number of non-zero entries is a small proportion of the matrix). It has a small, fixed number of parity equations checking each bit, and each parity equation checking the same number of bits. Gallager showed that such codes have good distance properties and that iterative computation of *a posteriori* probabilities for each bit could achieve a probability of bit error decreasing exponentially with block length. Recently, a practical and powerful iterative decoding based on the belief propagation method has been found [12]. With this decoding algorithm, some LDPC codes can achieve a remarkable error performance that is only a few tenth of a dB away

from Shannon's limit. Thus, these codes are very promising for many communication systems.

1.6 Overview

Practical CDMA cellular systems are very complicated. In order to evaluate the practical performance of these systems, we mainly used computer simulation techniques for link level evaluation and analytical methods for multicell environments. The simulators are based on IS-95 (which is currently in use) and IS-2000 CDMA systems and focus on the various methods for performance improvement like digital beamforming and coding techniques. We attempted to identify all the key factors in a practical situation and provide an analysis that is efficient, realistic and reliable.

Chapter 2 compares performances between adaptive antenna arrays and fixed multibeam systems for the reverse link of an IS-95 system. The adaptive beamforming method used is the recursive least squares (RLS) algorithm. A linear antenna array with four elements is assumed to be installed at the base station for the case of adaptive beamforming. The number of fixed beams for the multibeam situation is also four for comparison purposes. Chapter 3 investigates the possibility of applying LDPC codes to the forward link of IS-2000 systems. Their performance is compared with convolutional codes for various data rates. The digital beamforming and coding techniques are both evaluated based on chip

level simulations of the one cell CDMA system. Chapter 4 evaluates the performance of CDMA systems for a multicell environment. Because the computation work for link level simulations for this situation is exorbitant, an analytical model considering path loss, correlated log-normal shadowing and Rayleigh fast fading of signals and interferences is used for numerical evaluation. Also cell sectorizations of the cellular CDMA system are considered in this chapter.

The original contributions of this dissertation include the following:

- Comparing the performance of adaptive beamforming and fixed multibeam techniques for a realistic IS-95 CDMA system (Chap. 2).
- Applying LDPC codes to IS-2000 CDMA systems and comparing their performance with the convolutional and turbo codes (Chap. 3).
- Including correlated shadowing effects and cell sectorizations in an efficient analytical method for BER performance evaluation in multicell environments (Chap. 4).

Chapter 2

Antenna Performance Comparisons for IS-95 CDMA Systems

2.1 Introduction

Digital beamforming can increase both the performance and the capacity of CDMA systems. This is realized through antenna arrays deployed at the base stations. The antenna array with adaptive beamforming can steer the beam with the largest gain towards the desired user, and place nulls on the interferers, leading to suppressed interference and improved signal-to-noise ratio (SNR). A simpler approach is the switched multibeam antenna system. It uses several narrow beams to service the entire coverage of the base station. The beam that receives the desired signal with the highest signal strength is selected. This chapter compares the performance of adaptive antenna arrays and switched multibeam antenna techniques for the reverse link of IS-95 CDMA systems.

2.2 Simulation Procedure

2.2.1 IS-95 System Simulation

2.2.1.1 Transmitter Description

The reverse IS-95 CDMA channel structure that is considered in our simulation is shown in Fig. 2.1 [3].

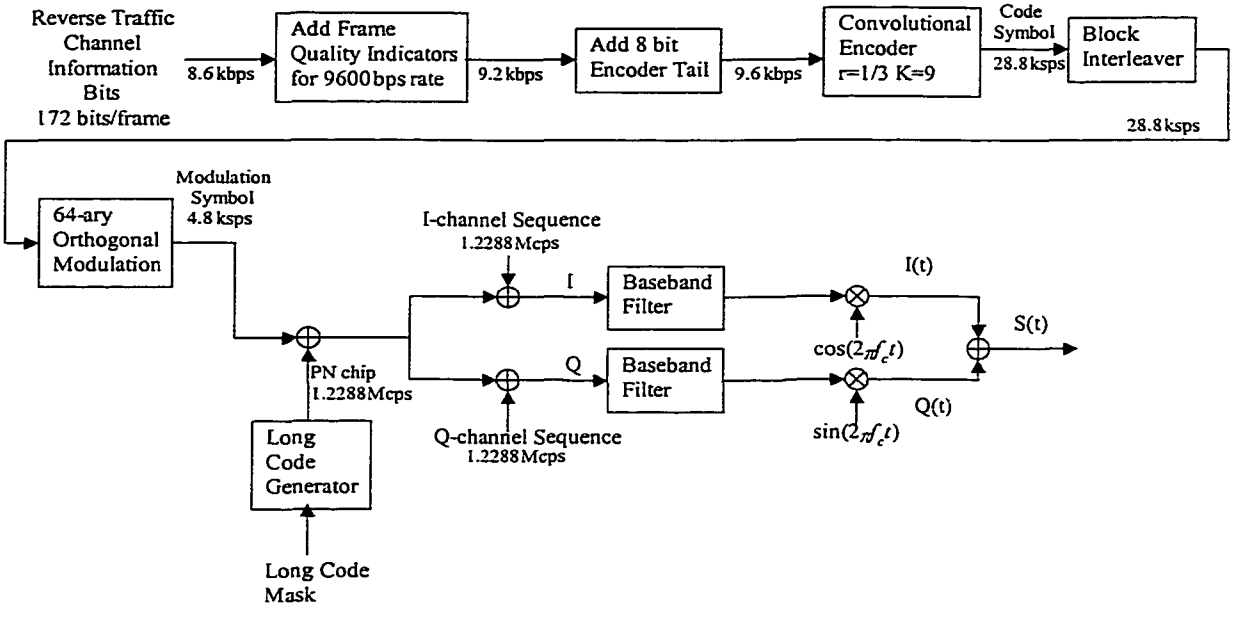


Fig. 2.1. Reverse CDMA channel structure.

For each 20 ms frame, 16 frame quality indicator bits and 8 encoder tail bits are added to 172 information bits. After that, these bits are encoded and block interleaved. Corresponding to each 6 code symbols, one of 64 possible modulation symbols is transmitted. They are multiplied by long PN code, I-

channel and Q-channel PN codes respectively. The resulted spread signal impulses are applied to the input of a pulse shaping filter and modulated by two quadrature carriers, so that a QPSK signal $s(t)$ is transmitted.

The details of the various components of the transmitter are as follows.

Frame Quality Indicator

Each 20 ms frame for 9.6 kb/s data rate includes a frame quality indicator. This frame quality indicator is a cyclic redundancy check (CRC) code. It is calculated on all bits within the frame, except the frame quality indicator itself and eight encoder tail bits, which are all zeros. The generator polynomial for this frame quality indicator is as follows:

$$g(x) = x^{12} + x^{11} + x^{10} + x^9 + x^8 + x^4 + x + 1. \qquad (2.1)$$

Convolutional Encoding

The convolutional code has rate 1/3 and a constraint length of 9. The generator function for this code is $g_0 = 557$ (octal), $g_1 = 663$ (octal), $g_2 = 711$ (octal) respectively.

Block Interleaving

20 ms block interleaver corresponds to an array with 32 rows and 18 columns. Code symbols are written into the interleaver by columns filling the complete 32×18 matrix and output from the interleaver by rows.

Orthogonal Modulation

64-ary orthogonal modulation is used for the reverse link of IS-95 systems. Each six code symbols correspond to one of 64 modulation symbols, which are mutually orthogonal waveforms generated using Walsh functions. Walsh functions can be generated in the following recursive manner:

$$H_1 = 0, \qquad H_2 = \begin{bmatrix} 0 & 0 \\ 0 & 1 \end{bmatrix}, \qquad H_{2N} = \begin{bmatrix} H_N & H_N \\ H_N & \overline{H}_N \end{bmatrix}, \tag{2.2}$$

where N is a power of 2 and $\overline{H}_N$ represents the binary complement of H_N.

PN Long Code Spreading

PN long code is periodic with a period of $2^{42}-1$ chips and satisfies the linear recursion specified by the following characteristic polynomial:

$$\begin{aligned} p(x) = {} & x^{42} + x^{35} + x^{33} + x^{31} + x^{27} + x^{26} + x^{25} + x^{22} + x^{21} + x^{19} + x^{18} \\ & + x^{17} + x^{16} + x^{10} + x^{7} + x^{6} + x^{5} + x^{3} + x^{2} + x^{1} + 1. \end{aligned} \tag{2.3}$$

Each PN chip of the long code is generated by the modulo-2 inner product of a 42-bit mask and the 42-bit state vector of the sequence generator. For different users, we randomly generate their respective masks.

Quadrature Spreading

In-phase (I) and quadrature-phase (Q) sequences are periodic with a period of 2^{15} chips. They are based on the following characteristic polynomials, respectively:

$$P_I(x) = x^{15} + x^{13} + x^{9} + x^{8} + x^{7} + x^{5} + 1, \tag{2.4}$$

and

$$P_Q(x) = x^{15} + x^{12} + x^{11} + x^{10} + x^6 + x^5 + x^4 + x^3 + 1. \qquad (2.5)$$

The products of the long code with in-phase and quadrature-phase sequences form the I and Q channel spreading sequences, respectively.

Baseband Filtering

The impulse response of baseband filter $p(t)$ is shown in Fig. 2.2.

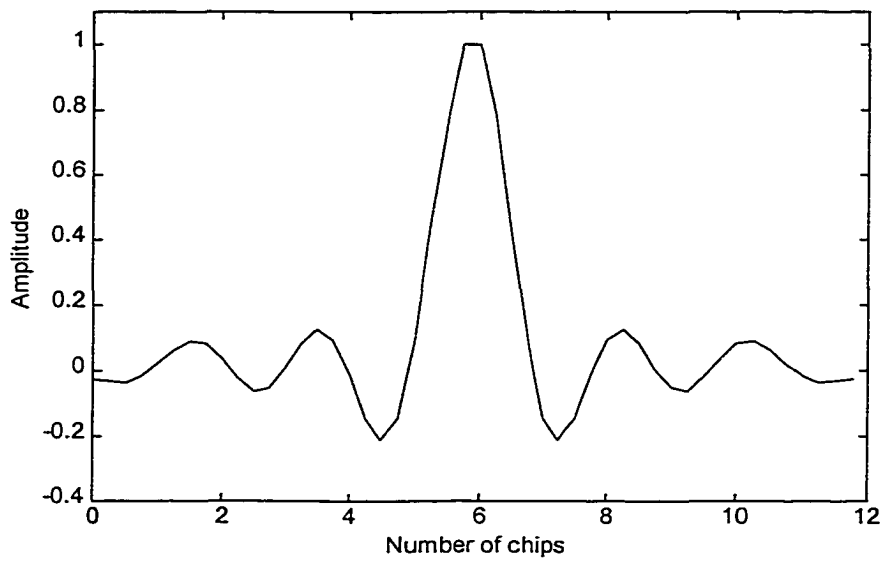


Fig. 2.2. Impulse response of baseband filter.

The PN chip rate is 1.2288 Mchips/s. The duration of the impulse response is 12 chip periods.

QPSK Signal Mapping

The mapping between the signal impulses and the carrier phases are shown in Table 2.1.

TABLE 2.1

QPSK SIGNAL MAPPING

I	Q	Phase
0	0	$\pi/4$
1	0	$3\pi/4$
1	1	$-3\pi/4$
0	1	$-\pi/4$

2.2.1.2 Channel Modeling

For the channel modeling, we use Jake's fading model to generate time-correlated Rayleigh fading waveforms [13]. Jake's fading model is a deterministic method for simulating time-correlated Rayleigh fading waveforms. In this model, fading is mainly influenced by the speed of the vehicle and the carrier frequency. Walsh-Hadamard codewords are used to generate uncorrelated waveforms for different users. Usually, if the vehicle speed is high, both the amplitude and the phase of the signal change relatively quickly. Fig. 2.3 shows the fast fading waveforms for vehicle speeds of 10 and 30 km/hr within one second period. We

can see from the figure that when the speed increases from 10 km/hr to 30 km/hr, the amplitude of the signal changes faster.

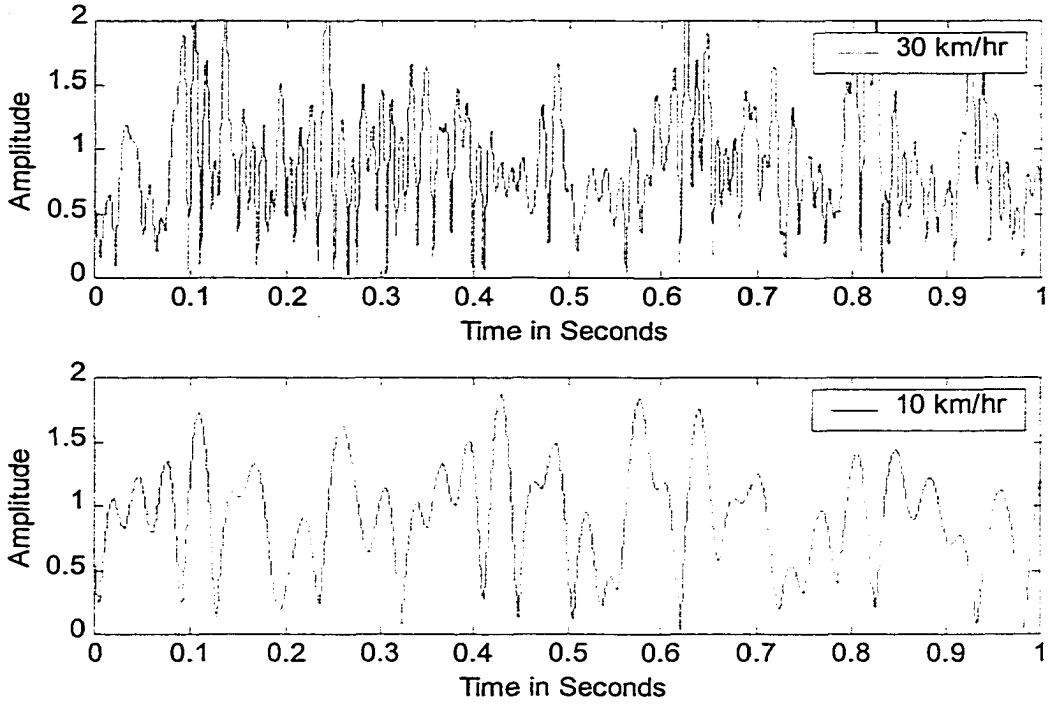


Fig. 2.3. Fast fading waveforms for speeds of 10 and 30 km/hr within one second period.

If we choose the carrier frequency f_c for the reverse link of IS-95 as 1.87×10^9 Hz and the vehicle speed v as 30 km/hr, then the corresponding Doppler frequency is

$$w = 2\pi f_c v / c = 326.6\,Hz, \tag{2.6}$$

where c is the speed of light. Using a sampling period of $208.33\,\mu s$, which is the modulation symbol period, and 1000000 samples, we can get the autocorrelation

function of the simulated Rayleigh waveforms as shown in Fig. 2.4, and they agree very well with theoretical results. Also, compared with the real part of autocorrelation function, the crosscorrelation between the real part and imaginary part of simulated fadings, which are represented by the imaginary part of autocorrelation function, is very small, as shown in Fig. 2.5.

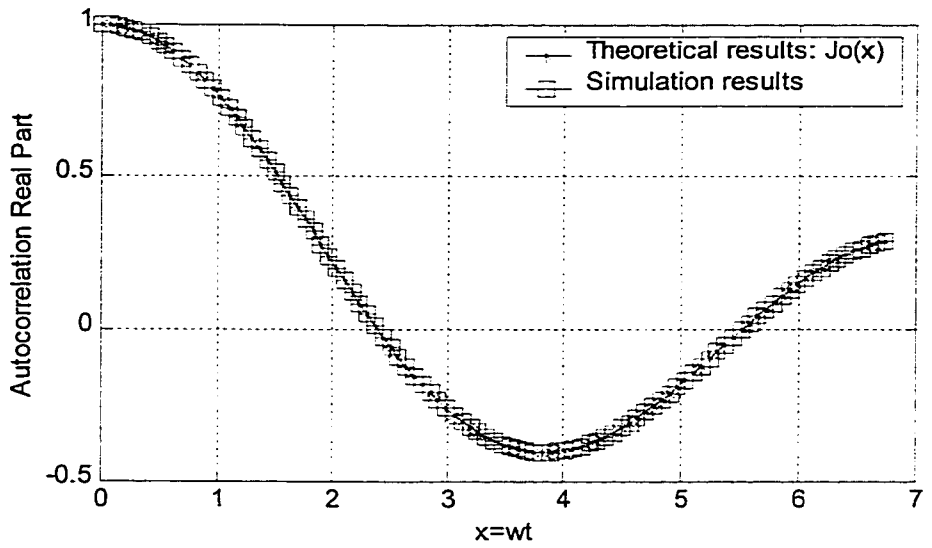


Fig. 2.4. Autocorrelation functions for both simulated and theoretical Rayleigh waveforms.

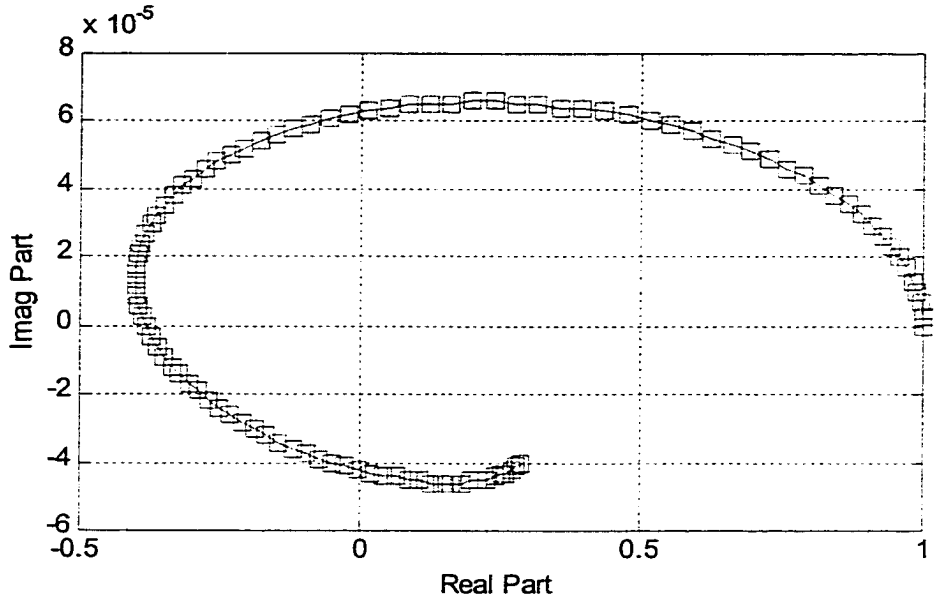


Fig. 2.5. Imaginary part versus real part of autocorrelation functions of simulated Rayleigh waveforms.

2.2.1.3. Receiver Description

We consider K users randomly distributed around a cell site at varying ranges. The first user is the desired user. Each user has only one multipath. The simulation model assumes that the asynchronous transmissions are chip synchronous (for convenience of simulation) and the receiver uses a non-coherent method to detect the modulation symbols.

Let $a_I^i(t)$ and $a_Q^i(t)$ denote the spreading waveforms of the I and Q channels for the i th user, respectively. $a_I^i(t)$ and $a_Q^i(t)$ are represented by [14]

$$a_I^i(t) = \sum_{h=-\infty}^{\infty} a_h^{I,i} p(t - hT_c),$$

$$a_Q^i(t) = \sum_{h=-\infty}^{\infty} a_h^{Q,i} p(t - hT_c), \tag{2.7}$$

where $a_h^{I,i}$ and $a_h^{Q,i}$ are the products of long PN code and short I, Q PN codes respectively. They take values +1 and −1. T_c is the chip duration, and $p(t)$ represents the time limited impulse response waveform shown in Fig. 2.2.

If we denote the fading of the channels as $\alpha_n e^{-j\theta_n}$, where α_n and θ_n are the amplitude and phase of the fadings respectively and n is the time index, then the channel output of the *ith* user is

$$\begin{aligned} y_i(t) = \sqrt{P_n^i}\alpha_n^i [W^i(t-\tau_n^i)a_I^i(t-\tau_n^i)\cos(\omega_c t + \theta_n^i) \\ + W^i(t - T_0 - \tau_n^i)a_Q^i(t - T_0 - \tau_n^i)\sin(\omega_c t + \theta_n^i)] \ , \end{aligned} \tag{2.8}$$

where P is the transmitted power per symbol, τ is the delay of the signal, T_0 is the time offset between the I and Q channels which is one half of chip period, and $W(t)$ is the Walsh orthogonal modulation symbol waveform. Thus, the signal at the input of the receiver becomes

$$
\begin{aligned}
r(t_n) &= \sum_{i=1}^{K} y_i(t_n) \\
&= [\sum_{i=1}^{K} \sqrt{P_n^i}\alpha_n^i W^i(t_n - \tau_n^i) a_I^i(t_n - \tau_n^i)\cos\theta_n^i + \\
&\sum_{i=1}^{K} \sqrt{P_n^i}\alpha_n^i W^i(t_n - T_0 - \tau_n^i) a_Q^i(t_n - T_0 - \tau_n^i)\sin\theta_n^i]\cos(\omega_c t_n) \\
&+ [-\sum_{i=1}^{K} \sqrt{P_n^i}\alpha_n^i W^i(t_n - \tau_n^i) a_I^i(t_n - \tau_n^i)\sin\theta_n^i + \\
&\sum_{i=1}^{K} \sqrt{P_n^i}\alpha_n^i W^i(t_n - T_0 - \tau_n^i) a_Q^i(t_n - T_0 - \tau_n^i)\cos\theta_n^i]\sin(\omega_c t_n) .
\end{aligned} \tag{2.9}
$$

So the complex low-pass equivalent expression is

$$
r(t) = x_I(t) + jx_Q(t) = (A + B) + j(C - D) , \tag{2.10}
$$

with

$$
\begin{aligned}
A &= \sum_{i=1}^{K} \sqrt{P_n^i}\alpha_n^i W^i(t_n - \tau_n^i) a_I^i(t_n - \tau_n^i)\cos\theta_n^i , \\
B &= \sum_{i=1}^{K} \sqrt{P_n^i}\alpha_n^i W^i(t_n - T_0 - \tau_n^i) a_Q^i(t_n - T_0 - \tau_n^i)\sin\theta_n^i , \\
C &= \sum_{i=1}^{K} \sqrt{P_n^i}\alpha_n^i W^i(t_n - \tau_n^i) a_I^i(t_n - \tau_n^i)\sin\theta_n^i , \\
D &= \sum_{i=1}^{K} \sqrt{P_n^i}\alpha_n^i W^i(t_n - T_0 - \tau_n^i) a_Q^i(t_n - T_0 - \tau_n^i)\cos\theta_n^i .
\end{aligned}
$$

Then the following carrier modulated signal

$$
\begin{aligned}
&[(A + B) + j(C - D)][\cos(\omega_c t) + j\sin(\omega_c t)] = \\
&(A + B)\cos(\omega_c t) - (C - D)\sin(\omega_c t) + j \cdot [(A + B)\sin(\omega_c t) + (C - D)\cos(\omega_c t)]
\end{aligned} \tag{2.11}
$$

is demodulated by $\cos(\omega_c t)$ and $\sin(\omega_c t)$ at the receiver respectively (Fig. 2.6 [15]). The output of the low-pass filter of the I and Q channel is

$$
\begin{aligned}
d_I(t) &= (A + B)/2, \\
d_Q(t) &= -(C - D)/2 .
\end{aligned} \tag{2.12}
$$

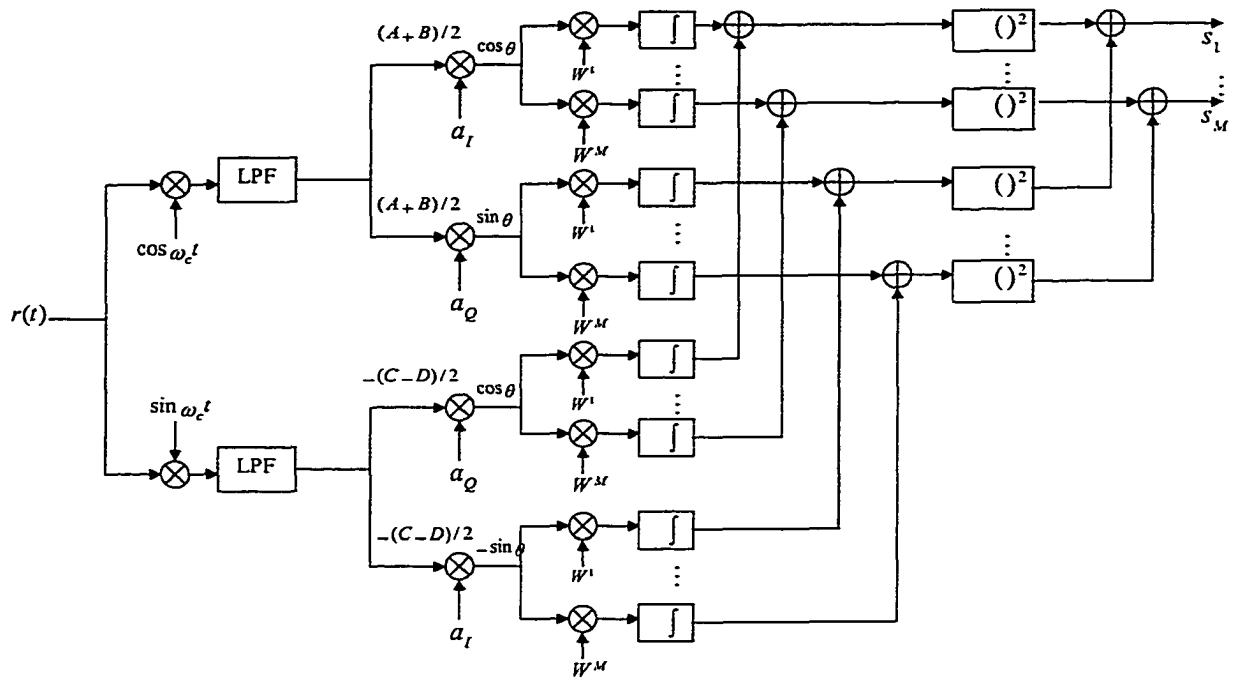


Fig. 2.6. Schematic diagram of non-coherent detection procedure.

If we define

$$
\begin{aligned}
d_{II}(t) &= d_I(t)a_I^1(t-\tau_n^1), \\
d_{IQ}(t) &= d_I(t)a_Q^k(t-T_0-\tau_n^1), \\
d_{QI}(t) &= d_Q(t)a_I^k(t-\tau_n^1), \\
d_{QQ}(t) &= d_Q(t)a_Q^k(t-T_0-\tau_n^1),
\end{aligned}
\tag{2.13}
$$

then, the output of the correlator for one of the 64 possible Walsh orthogonal functions, which is denoted as the m th function, is defined as

$$Z_{II}(m) = \frac{1}{\sqrt{T_w}} \int_{\tau_n^1}^{T_w+\tau_n^1} d_{II}(t) W_m^1(t-\tau_n^1)dt,$$

$$Z_{IQ}(m) = \frac{1}{\sqrt{T_w}} \int_{\tau_n^1+T_0}^{T_w+\tau_n^1+T_0} d_{II}(t) W_m^1(t-\tau_n^1-T_0)dt,$$

$$Z_{QI}(m) = \frac{1}{\sqrt{T_w}} \int_{\tau_n^1}^{T_w+\tau_n^1} d_{QI}(t) W_m^1(t-\tau_n^1)dt,$$

$$Z_{QQ}(m) = \frac{1}{\sqrt{T_w}} \int_{\tau_n^1+T_0}^{T_w+\tau_n^1+T_0} d_{QQ}(t) W_m^1(t-\tau_n^1-T_0)dt, \qquad (2.14)$$

where T_W is the modulation symbol period. Then the decision variables of the desired user are

$$S(m) = [Z_{II}^k(m) + Z_{QQ}^k(m)]^2 + [Z_{IQ}^k(m) - Z_{QI}^k(m)]^2, \quad m = 1,2,\cdots,64. \qquad (2.15)$$

The Walsh function with the largest value of the decision variables is chosen as the transmitted symbol. The receiver uses these decision variables for the estimation of the short-term average symbol energy to noise ratio E_s / N_0 and *a posteriori* probabilities of code symbols for the decoder.

2.2.1.4 Power Control Techniques

Closed Loop Power Control (CLPC) is used for the base station to command the mobile to adjust its transmit power based on the reverse link received SNR. CLPC is comprised of two parts: the inner (fast) loop and the outer (slow) loop. The inner loop assumes knowledge of a target energy-per-bit to interference density ratio, E_b / I_o, and the base station sends increase/decrease transmit power

commands to the mobile station to assist reaching that target. The outer loop, on the other hand, is responsible for setting the target E_b / I_o. In our system, the inner loop updates take place every 1.25 ms, while the outer loop updates are once per every 20 ms frame.

Outer loop power control [16]

The algorithm for adjusting the target E_b / I_o, is as follows. First, use CRC to check if current frame is in error. In our simulations, if the calculated frame quality indicator is {1,0,1,0,0,0,1,0,1,0,1,1}, then we say the frame is correct, if not, the frame is in error. Whenever we determine from the frame quality indicator that the current frame is in error, then the outer loop power control scheme will increase E_b / I_o by a larger step $K\Delta$, where Δ is the step size in dB and $K \geq 1$ is an integer. On the other hand, if the frame quality indicator indicates that the current frame is correct, E_b / I_o will be decreased by a smaller step like Δ. In this way, the frame error rate of the system will be controlled. The algorithm aims to keep the FER always less than or equal to $1/(K+1)$.

Inner loop power control [17]

Since the decoder has large delay due to deinterleaving, information to be used for feedback power control must be extracted before deinterleaving. We have the following simple way for estimating the short-term average symbol energy to noise ratio E_s / N_o.

For the desired user, if we define the jth consecutive Walsh symbol non-coherent detection output as $S(m, j)$, then we have

$$\frac{\hat{E}_s}{N_o} = \frac{1}{N_w}\sum_{j=1}^{N_w}\frac{max\{S(1,j), S(2,j)\cdots S(M,j)\}}{\sum_{m\neq max} S(m,j)}, \tag{2.16}$$

where N_w is the number of modulation symbol periods, which is the window length of the short-term average. The estimated E_s / N_o is used through the inner power control loop by the mobile power control block to determine whether to increase or decrease the mobile transmit power. In our simulation, $N_w = 6$.

2.2.1.5 Soft Output Decision Decoding (SOVA)

In this decoding process, the decision variables $S(m)$ in (2.15) are used to derive the input bit likelihood ratio for every coded symbol b_n. The likelihood ratio is defined to be:

$$\begin{aligned} L(b_n) &= \frac{Joint\ pdf\ of\ (S(1), S(2), \cdots, S(64)/b^n = 0)}{Joint\ pdf\ of\ (S(1), S(2), \cdots, S(64)/b^n = 1)} \\ &= \frac{\sum_{m=1}^{64}\delta_{m,0}^n I_0(2\sqrt{S(m)\frac{E_s}{N_o}})}{\sum_{m=1}^{64}\delta_{m,1}^n I_0(2\sqrt{S(m)\frac{E_s}{N_o}})}, \end{aligned} \tag{2.17}$$

where

$$\delta_{m,x}^n = \begin{cases} 1 & if\ nth\ bit\ of\ the\ mth \\ & input\ vector\ is\ equal\ to\ x, \\ 0 & otherwise, \end{cases}$$

and the estimated E_s / N_o shown in (2.16) is used in the simulation. The output of the deinterleaver, to be input to the Viterbi decoder, is the sequence of $L(b_n)$. The soft-decision metric for the j-th branch of the r-th path is expressed as

$$\mu_n^{(r)} = (1-2b_n^{(r)}) \cdot log(L(b_n^{(r)})). \tag{2.18}$$

By using the above equation, the Viterbi decoder calculates the accumulated path metrics

$$U^{(r)} = \sum_{n=1}^{B} \mu_n^{(r)} = \sum_{n=1}^{B} (1-2b_n^{(r)}) \cdot log(L(b_n^{(r)})), \tag{2.19}$$

and keeps the path with the largest value.

2.2.2 Adaptive Antenna Arrays

We consider one sector and a 4-element uniform linear array (ULA) with interelement spacing denoted as d at the base station as shown in Fig. 2.7. If we assume the signal comes at an angle θ, then the phase lead of the signal at element i $(i \geq 1)$ relative to that at element 1 is $\kappa(i-1)d\,sin\theta$, where $\kappa = 2\pi / \lambda$ and λ is the wavelength of the signal. Then we have the array propagation vector which is defined as

$$\zeta = [1 \quad e^{j\kappa d sin\theta} \quad e^{j2\kappa d sin\theta} \quad e^{j3\kappa d sin\theta}]^T. \tag{2.20}$$

The angle of arrival of the signal is reflected in its array propagation vector. The combined effect of the array propagation vector and complex weights for each of four elements will steer the output beam towards the desired direction.

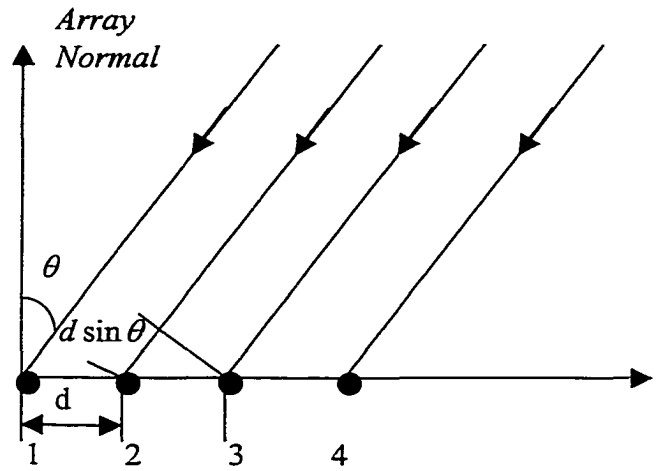


Fig. 2.7. Four element uniform linear array.

The adaptive algorithm we use in our simulations is the RLS algorithm. The main idea of the RLS algorithm is to recursively perform the matrix inversion so that the direct matrix inversion is no longer required. It employs a Kalman gain vector that is computed from the current and previous received signal. This will lead to a faster convergence than the least mean square (LMS) algorithm that only uses the current received signal information for weight vector update.

Following are the details for the RLS algorithm. It is used to find a weight vector (w_1, w_2, w_3, w_4) such that the array can steer a beam in a desired direction. For the antenna arrays at the base station, if we assume the received signal is $r(n)$, then we denote

$$x(n) = r(n) \cdot \zeta = [r(n) \quad r(n)e^{j\kappa d\sin\theta} \quad r(n)e^{j2\kappa d\sin\theta} \quad r(n)e^{j3\kappa d\sin\theta}]^T,$$

$$A_n = \begin{bmatrix} \beta^{n-1} & 0 & \cdots & 0 \\ 0 & \beta^{n-2} & \cdots & 0 \\ \vdots & \vdots & \ddots & 0 \\ 0 & 0 & \cdots & 1 \end{bmatrix},$$

$$P^{-1}(n) = x^{T}(n) A_n^{-1} x^{*}(n), \tag{2.21}$$

where β is the forgetting factor. Then, the iterative relations [18] are

$$P(n+1) = \frac{1}{\beta}\left\{P(n) - \frac{P(n)x^{*}(n+1)x^{T}(n+1)P(n)}{\alpha + x^{T}(n+1)P(n)x^{*}(n+1)}\right\},$$

$$w(n+1) = w(n) + \frac{P(n)x^{*}(n+1)}{\beta + x^{T}(n+1)P(n)x^{*}(n+1)}\left[ref(n+1) - w^{T}(n)x(n+1)\right], \tag{2.22}$$

where $ref(n)$ is a desired reference signal. Equation (2.22) is started by adopting an initial guess for the weight vector $w(0)$ and the initial Hermitian matrix $P(0)$. It is common practice to select as an initial weight vector $w(0) = [1,0,0,0]$, thereby obtaining an omni-directional array pattern (the antenna elements each have omni-directional patterns) and to select $P(0)$ as the identity matrix. The adaptive array output signal $z(n)$ can be written as

$$z(n) = w^{T}(n)x(n). \tag{2.23}$$

The reference signal $ref(n)$ is obtained by re-modulating the non-coherent output through mixing with the corresponding spreading sequencies. The re-modulated signal is used as the reference signal for the RLS algorithm (In the simulations, we assumed perfect knowledge of the transmitted symbols).

In one of our simulation examples, we consider a four-element antenna array and assume the angles of arrival of four users to be 0.0, -1.0, -0.5 and 0.5 rads respectively. We got the convergence weight vectors and the array beam pattern shown in Figs. 2.8 and 2.9, respectively. We can see from Fig. 2.8 that the absolute values of the weight vectors for four antenna elements converge after approximately 20 chips. In Fig. 2.9, the angle of arrival of the desired user is 0.0 rad. Notice that the adaptive array has steered the beam in the desired direction and placed nulls in the directions of the interference arrivals.

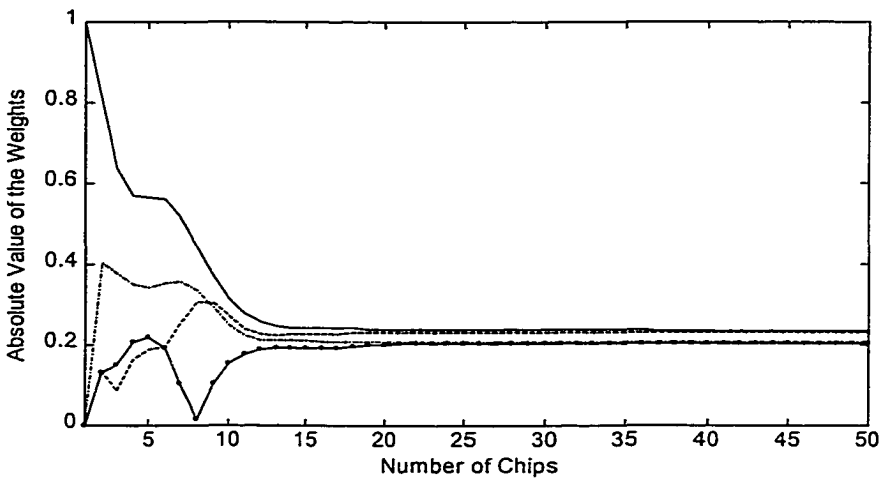


Fig. 2.8. The convergence of the RLS adaptive array with fixed angle of arrival for the desired user.

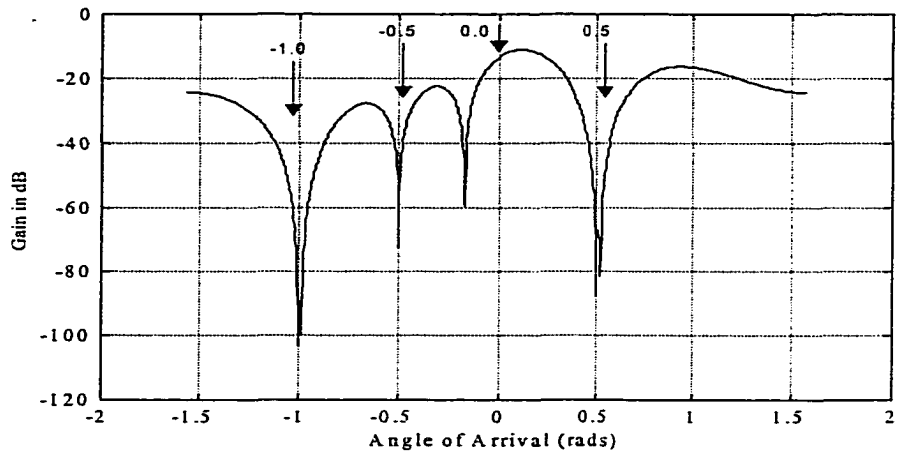


Fig. 2.9. Array beam pattern using RLS for four users with angles of arrival 0.0, -1.0, -0.5, 0.5 rads.

2.2.3. Switching Beam Antennas

For the fixed beam antenna [19], the 120° sector is being covered by four narrow beams each with 30° half-power beamwidth (Fig. 2.10). In our simulations, the signal transmitted from each subscriber is received by each of the fixed narrow beams. The proper beam is selected according to the estimated short-term average E_s / N_o in (2.16). It is assumed that the estimated short-term average E_s / N_o received by the proper beam is larger than that received by any other beam.

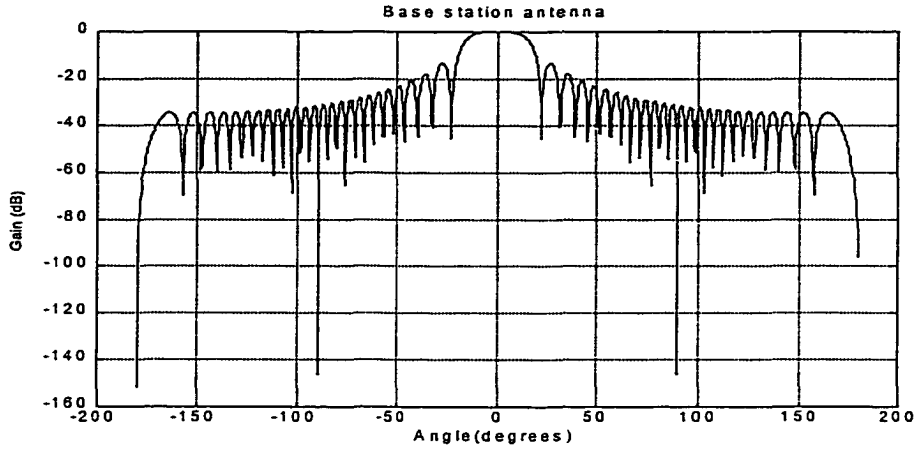


Fig. 2.10. Array beam pattern with 30° beamwidth (HPBW).

2.3 Simulation Assumptions and Results

For the IS-95 system validation, the reverse link FER simulation was carried out according to the setting parameters shown in Table 2.2 [20]. We used Gaussian approximation for the interferences in our validation.

In our validation, we took four samples per chip, and used the following two ways to estimate E_b/N_o:

1. The simulator knows the transmitted power P of the user, so

$$\frac{E_b}{N_o} = \frac{2*P*3.9403}{2*\sigma^2} * 128, \qquad (2.24).$$

where σ is the variance of Gaussian noise for the I and Q channel, 3.9403 is the sum of squares of coefficients of the pulse shaping filter in Fig. 2.2. Or we used the accumulated average energy of the samples both for the desired signal E and Gaussian noise N at the receiver,

$$\frac{E_b}{N_o} = \frac{E}{N} * 4 * 128. \tag{2.25}$$

TABLE 2.2

SETTING PARAMETERS FOR THE VALIDATION

Parameter	**Data**	**Units**
Carrier Frequency	1870	MHz
Information Bit Rate	9600	bps
Information Bit Source	Random	
FEC Code Rate	1/3	
Fading	Rayleigh	
Vehicle Speed	1,8,30,100, and 160	km/hr
Closed-Loop Power Control	On, with 4% error rate on the control bits	
Outer-Loop Power Control	Off ($E_b/(N_o+I_o)$) set point fixed	
Rate Determination	Assumed perfect	
No. of Paths (Fingers)	Fixed at 1	

2. Without knowing the transmitted power of the user, the simulator gets the estimated E_b / N_o simply by dividing the estimated E_s / N_o in (2.16) by 2.

Our validation results are shown in Tables 2.3 and 2.4.

TABLE 2.3

REQUIRED E_b/N_o AT A FIXED FER WITH NO FADING

Channel	Non-fading					
Power Control	Off		On, 0% BER		On, 4% BER	
Estimation Method	1	2	1	2	1	2
Req. E_b/N_o for 10% FER	4.5	5.0	4.9	5.4	4.9	5.4
Req. E_b/N_o for1% FER	5.1	5.4	5.6	5.9	5.8	6.1

TABLE 2.4

REQUIRED E_b/N_o AT A FIXED FER WITH ONE FADING PATH

Channel	Fading									
Power Control	On, 4% BER									
Mobile Speed (km/hr)	1		8		30		100		160	
Estimation Method	1	2	1	2	1	2	1	2	1	2
Req. E_b/N_o for10% FER	5.2	5.6	7.7	8.0	8.4	8.7	7.9	8.2	7.6	8.0
Req. E_b/N_o for 1% FER	6.1	6.3	N/A	N/A	N/A	N/A	9.8	9.9	9.1	9.3

The differences between our results and Qualcomm's results are within 0.6 dB for the evaluation method with knowledge of transmitted power and 0.8 dB for the method with estimated E_s/N_o.

To compare the performance between adaptive antenna arrays and fixed multibeam techniques, we use the initial parameters in Table 2.5.

TABLE 2.5

INITIAL CONDITIONS FOR THE SIMULATION SCENARIO

Parameter	Data	Units
Number of users	4,10,20,30	
Distance to Base station	500	m
Radius of the Moving Area	1.0	km
Moving Speeds	1,8,30,100,160	km/hr
Changing Frequency of Angle of Moving Directions	2	s

We considered four 30° beams in a 120° sector for the fixed multibeam system, and four antenna elements in the sector for the RLS case. The desired user and the interferers (we considered one desired user with 3, 9 and 29 interferers respectively) are moving randomly in the sector with the same speed (we consider 1, 8, 30, 100 and 160 km/hr speeds respectively). Perfect power control is assumed for all the interferers, but not for the desired user. Results are based on a fixed 10% or 1% FER, which is controlled by the outer loop power control

method, and the input signal to interference ratio (SIR) is being measured before beamforming for both cases. We choose the initial location of the users to be always in favor of the switching multibeam configuration, i.e., the angle of arrival of the desired user coincides with the largest antenna gain. Because the users keep on moving in our simulation scenarios, the input SIR will not converge. In order to make a fair comparison, we use the average input SIR calculated till the time of the 1000^{th} reliable frame for 10% FER and 10000^{th} reliable frame for 1% FER for comparison purposes. If the speed is high, e.g., 160 km/hr, the total change in angle of arrival before we stop the simulation is much larger than for the low speed case, e.g., 1 km/hr. The initial conditions for RLS and the fixed multibeam system are the same.

For four users (one desired user and three interferers) and 10% FER, the results depend heavily on the initial positions of the users considered (refer to Table 2.6, Figs. 2.11 and 2.12). We can see from Fig. 2.11 that for all speeds, RLS performs much better than the fixed multibeam configuration. The reason is very clear if we look at their beam patterns shown in Fig. 2.12.

TABLE 2.6

REQUIRED INPUT SIR FOR FOUR USERS AND 10% FER

Speed (km/hr)	1	8	30	100	160
Required Input SIR for RLS (dB)	-70.9	-69.7	-68.0	-65.9	-35.4
Required Input SIR for Fixed Multibeam (dB)	-16.1	-22.1	-23.0	-25.5	-17.4

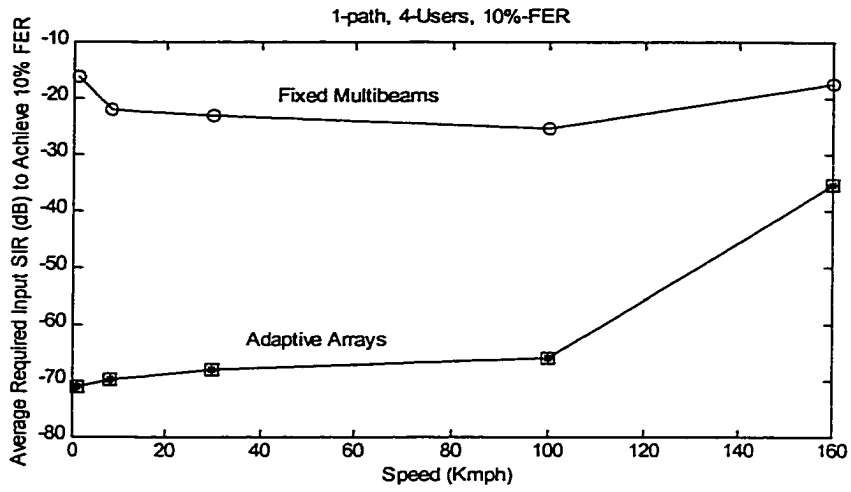


Fig. 2.11. Comparison between adaptive arrays and fixed multibeam for four users and 10% FER.

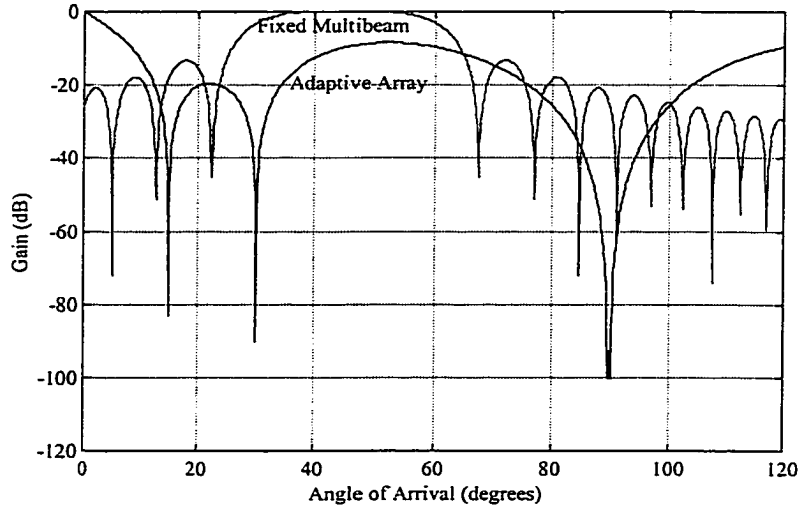


Fig. 2.12. Beampattern comparisons between adaptive arrays and fixed multibeam for four users and 10% FER.

The angle of arrival of the desired user is 45°; the angles of arrival of the interferers are 15°, 30° and 90° respectively. We can see from the beampatterns, that the adaptive array can steer the large beam to the desired users, and place nulls on the interferers. Also, the fixed multibeam technique can select the appropriate fixed beam for the desired user. Because three interferers can be completely suppressed by four antenna elements, the adaptive array has superior performance over the fixed multibeam.

As the number of interferers increases, the situation is a little more complicated. Table 2.7, Figs. 2.13 and 2.14 present the simulation results for ten users at 10% FER. Fig. 2.13 shows that for both lower and higher speeds, the adaptive antenna array still performs better than the fixed multibeam, but for the speeds in between, the fixed multibeam seems to be better. We can see from the beampatterns shown in Fig. 2.14 that for ten users, the adaptive antenna can still steer a large beam to the desired user, but it cannot place nulls on all interferers any longer. Because of the interactions between those users, the beampattern is not looking as good as the one shown in Fig. 2.12 for four users. The performance of the adaptive array is comparable to the fixed multibeam in this situation.

TABLE 2.7

INPUT SIR FOR TEN USERS AND 10% FER

Speed (km/hr)	1	8	30	100	160
Required input SIR for RLS(dB)	-21.1	-19.4	-18.2	-18.4	-20.4
Required input SIR for Sectorizatoin(dB)	-13.8	-19.7	-19.6	-17.9	-18.1

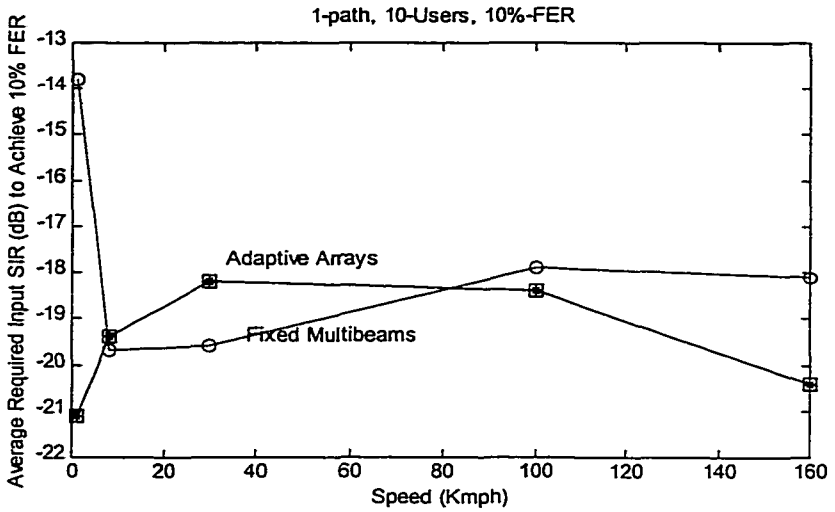


Fig. 2.13. Comparison between adaptive arrays and fixed multibeam for ten users and 10% FER.

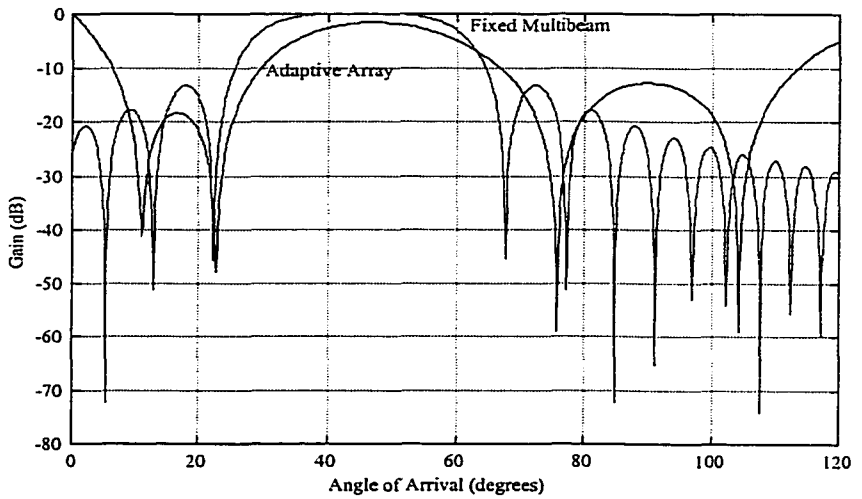


Fig. 2.14. Beampattern comparisons between adaptive arrays and fixed multibeam for ten users and 10% FER.

We also did simulations for twenty users at 10% FER. We can see from Table 2.8 and Fig. 2.15 that for speeds lower than approximately 50 km/hr, the adaptive array performs better than the fixed multibeam, but for higher speeds, the fixed multibeam shows superior performance over the adaptive antenna array.

TABLE 2.8

INPUT SIR FOR TWENTY USERS AND 10% FER

Speed (km/hr)	1	8	30	100	160
Required input SIR for RLS(dB)	-21.6	-19.6	-19.1	-16.5	-17.0
Required input SIR for Sectorizatoin(dB)	-20.9	-19.2	-17.6	-19.8	-18.9

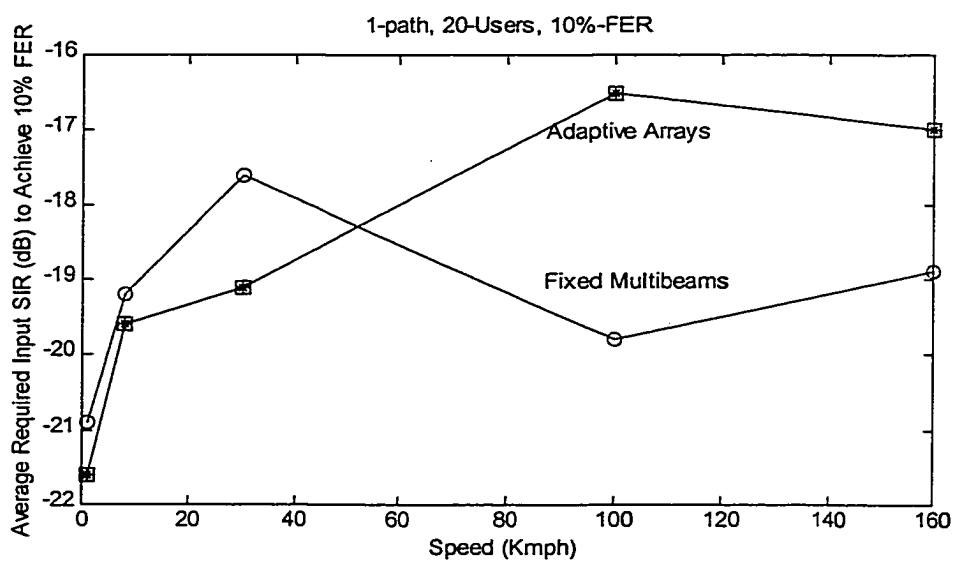


Fig. 2.15. Comparison between adaptive arrays and fixed multibeam for twenty users and 10% FER.

The situation is similar for thirty users at 1% FER, which is shown in Table 2.9, and Figs. 2.16 and 2.17. For each point in Fig. 2.16, we have run 10,000 frames. It is also the case here, that for lower speeds, these two schemes have comparable performance, but at higher speeds, the fixed multibeam is much better. Fig. 2.17 shows their beampatterns. We can see that even for thirty users, the adaptive array can still steer a larger beam to the desired user. But because the adaptive array has only four antenna elements it cannot null out all interferers. In addition, its tracking ability decreases very quickly compared with the fixed multibeam as the speeds become higher. The fixed mutibeam system outperforms the adaptive array under these conditions.

TABLE 2.9

REQUIRED INPUT SIR FOR THIRTY USERS AND 1% FER

Speed (km/hr)	1	8	30	100	160
Required Input SIR for RLS(dB)	-19.9	-16.3	-15.8	-12.2	-13.6
Required Input SIR for Sectorizatoin(dB)	-16.8	-15.6	-15.3	-16.8	-16.1

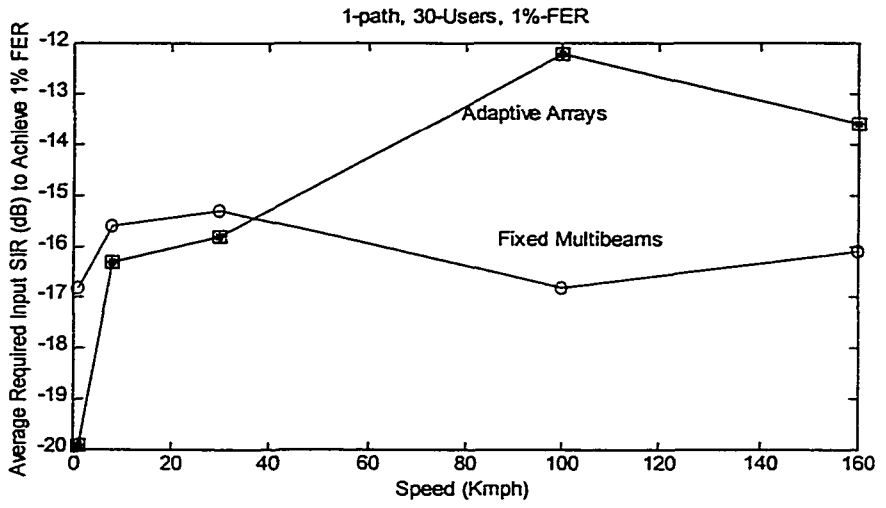


Fig. 2.16. Comparison between adaptive arrays and fixed multibeam for thirty users and 1% FER.

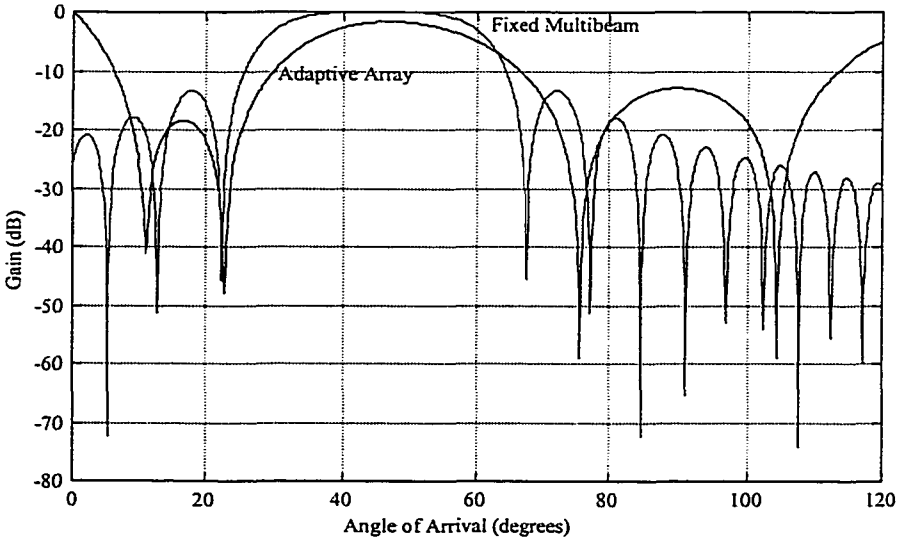


Fig. 2.17. Beampattern comparisons between adaptive arrays and fixed multibeam for thirty users and 1% FER.

2.4 Conclusions

From our simulation results, we can see that adaptive antenna arrays outperform the switching multibeam system in an interference-dominated situation if the number of interferers is relatively small and the speed is relatively low. A four element adaptive array can easily null out three interferers without any difficulty. In this situation, the adaptive antenna array has superior performance over a fixed multibeam regardless of the speeds of the users. If the number of interferers increases, the adaptive array cannot null out all the interferers, but it can always steer its beam to the direction of the desired user. Of course in our RLS adaptive array system, we rely on a perfect reference signal. In a realistic situation, however, we depend on the inherent correlation of the channel and the assumption that the channel remains almost constant over several symbol periods. In this case, the receiver can use a delayed estimation of the channel vector and the optimum beamforming weight vector. If an error occurs, the incorrect reference signal for the update of the weight vector will introduce severe performance degradation. Therefore, it is extremely important for the adaptive array system to avoid this mispointing error. For IS-2000 CDMA systems, however, there is always a pilot channel accompanying every traffic channel for the reverse link. In this situation, we will have a reliable reference signal for the adaptive antenna array.

If both the number of interferers and the speeds are very high, the RLS algorithm will no longer generate a meaningful beampattern. At that time, switching

multibeam methods will outperform adaptive arrays, because once the correct beam is selected, the beam pattern will not get worse with an increasing number of interferers. The fixed multibeam system can still track the users with a large number of interferers and with high speeds, while the adaptive array cannot.

Chapter 3

Low-Density Parity-Check Codes for IS-2000 CDMA Systems

3.1 Introduction

Powerful channel coding is a major requirement for third generation CDMA systems. The current IS-2000 standard already includes convolutional coding and turbo coding [4]. LDPC codes are error-correcting codes, which are defined by sparse parity-check matrices and can be decoded using iterative probabilistic algorithms. LDPC codes can achieve performance comparable to turbo codes on additive white Gaussian noise (AWGN) channels [21]. Motivated by their outstanding performance, we investigate the possible use of randomly generated LDPC codes with different codeword sizes in the forward link of an IS-2000 CDMA system over time correlated Rayleigh fading channels, and compare their performance with turbo and convolutional codes, which are part of the current standard.

3.2 System Modeling

In order to provide a fair comparison, we evaluate the performance of IS-2000 systems incorporating convolutional codes, turbo codes and LDPC codes respectively [22]. Fig. 3.1 [4] shows various components of the transmitter at the base station. At the transmitter, for each 20 ms frame, the information bits are encoded and block interleaved. After the power control bits are punctured, the coded and interleaved bits are split into two parallel streams (Y_I and Y_Q). They are spread with a Walsh orthogonal function at a fixed chip rate of 1.2288 Mcps and multiplied by a base station specific pseudo-random scrambling PN sequence.

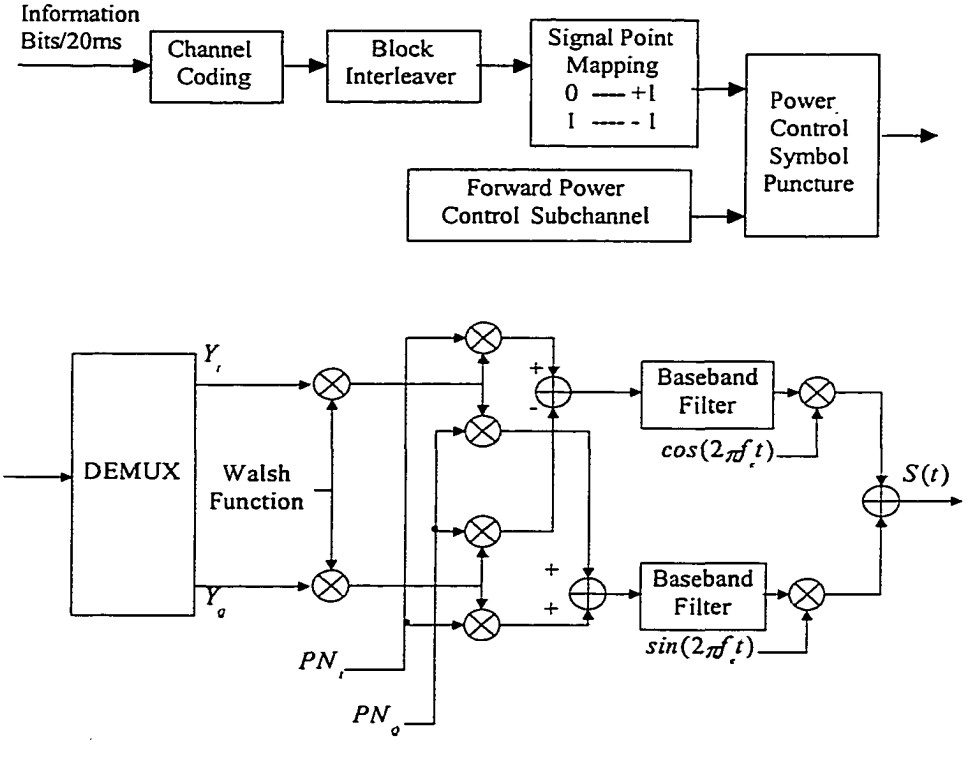


Fig. 3.1. IS-2000 forward link.

The resulting signals are applied to the input of pulse shaping filters and modulated by two quadrature carriers to generate a QPSK modulated signal $S(t)$. At the receiver, we use coherent detection and essentially perform the reverse operations of the transmitter. The following are various components of the system which are different from components in the reverse link of IS-95 system which was described in Chapter 2.

Block Interleaving

A block interleaver spanning 20 ms is used. The symbols input to the interleaver are written sequentially at addresses 0 to the block size (N) minus one. The interleaved symbols are read out in permutated order from address A_i as follows:

$$A_i = 2^m (i \bmod J) + BRO_m(\lfloor i/J \rfloor), \tag{3.1}$$

where

$i = 0$ to N-1,

$\lfloor x \rfloor$ indicates the largest integer less than or equal to x, and $BRO_m(y)$ indicates the bit-reversed m-bit value of y. The interleavers we have used in our simulation have the following parameters respectively.

TABLE 3.1

INTERLEAVER PARAMETERS

N	m	J
768	6	12
1536	6	24
3072	6	48
6144	7	48
12288	7	96

Power Control Subchannel

Within a 20 ms frame, we have 16 power control groups. In our simulation, the power control bits beginning positions are generated randomly within each group. For each power control bit, we punctured 4 symbols for 9.6 kb/s data rate.

Orthogonal Spreading

Each code channel transmitted on the forward CDMA channel is spread with a Walsh function at a fixed chip rate of 1.2288 Mcps.

Transmitted Signal for Traffic Channel

The transmitted signal for traffic channel within one symbol period is simply expressed as

$$s_t(t) = \sqrt{P_t} \cdot W_t(t) \cdot (Y_I \cdot PN_I(t) - Y_Q \cdot PN_Q(t)) \cdot \cos(2\pi f_c t) + \sqrt{P_t} \cdot W_t(t) \cdot (Y_I \cdot PN_Q(t) + Y_Q \cdot PN_I(t)) \cdot \sin(2\pi f_c t), \quad (3.2)$$

where P_t is transmitted power per symbol, where subscript t denotes the traffic channel. $W(t)$ is the Walsh code waveform; Y_I, Y_Q are the I and Q channel symbols respectively; PN_I and PN_Q are the PN sequences, and f_c is the carrier frequency of the signal.

Transmitted Signal for the Pilot Channel

The transmitted signal for the pilot channel within one symbol period is

$$s_p(t) = \sqrt{P_p} \cdot W_p(t) \cdot Y_I \cdot PN_I(t) \cdot \cos(2\pi f_c t) + \sqrt{P_p} \cdot W_P(t) \cdot Y_I \cdot PN_Q(t) \cdot \sin(2\pi f_c t). \quad (3.3)$$

where the subscript p denotes the pilot channel.

Receiver Description

We consider coherent detection at the receiver. The received signal at the receiver is

$$r(n) = (\sqrt{P_t} \cdot W_t(n) \cdot (Y_I \cdot PN_I(n) - Y_Q \cdot PN_Q(n)) + \sqrt{P_p} \cdot W_P(n) \cdot Y_I \cdot PN_I(n) - j\sqrt{P_p} \cdot W_P(n) \cdot Y_I \cdot PN_Q(n) - j\sqrt{P_t} \cdot W_t(Y_I \cdot PN_Q + Y_Q \cdot PN_I)) \cdot \alpha \cdot e^{j\theta} + N(t), \quad (3.4)$$

where $\alpha e^{j\theta}$ is the Rayleigh fading parameter generated by Jake's fading model [13] and $N(t)$ denotes a Gaussian random process. Thus, for the pilot channel, we have the following despread output

$$U_{dp} = \sum_{n=1}^{M} r(n) \cdot W_p(n) \cdot Y_I \cdot (PN_I(n) + j \cdot PN_Q(n))$$
$$= 2 \cdot M \cdot \sqrt{P_p} \cdot \alpha \cdot e^{j\theta} + N_{dp}. \quad (3.5)$$

So the estimated channel parameter is:

$$\hat{\alpha} \cdot e^{j\hat{\theta}} = U_{dp} / (2 \cdot M \cdot \sqrt{P_p}). \quad (3.6)$$

For the traffic channel, we have

$$U_{dt} = \sum_{n=1}^{M} r(n) \cdot W_t(n) \cdot \hat{\alpha} \cdot e^{-j\hat{\theta}} \cdot (PN_I(n) + j \cdot PN_Q(n)). \quad (3.7)$$

With perfect channel estimation, i.e.,

$$\hat{\alpha} \cdot e^{j\hat{\theta}} = \alpha \cdot e^{j\theta}, \quad (3.8)$$

we have

$$U_{dt} = 2 \cdot \alpha^2 \cdot \sqrt{P_t} \cdot (Y_I - j \cdot Y_Q) + N_{dt}. \quad (3.9)$$

Power Control Algorithm

We also consider both the inner loop and the outer loop power control scheme for the forward link of the IS-2000 system as we did for the reverse link of the IS-95 system in Chapter 2. Only this time the inner loop uses a different way to estimate the short term SNR [23].

The total interference and thermal noise or $N(t)$ is estimated by measuring the variation on the pilot channel:

$$\hat{N}(k) = F\left[\left|U_{dp}(k) - U_{dp}(k-1)\right|^2\right], \quad (3.10)$$

where $F[\cdot]$ is a non-causal moving average filter, and

$$\hat{E}_{pilot}(k) = U_{dp}(k) * U_{dp}^{*}(k). \tag{3.11}$$

Then we use the following way to estimate the pilot-to-traffic channel power ratio:

$$\frac{E_b}{E_{pilot}}(k) = \left[\frac{\left| U_{dt}(k) * U_{dt}^{*}(k) \right|}{U_{dp}(k) * U_{dp}^{*}(k)} \right]^2, \tag{3.12}$$

and

$$\left(\frac{E_b}{N} \right)_{measured} = \frac{\hat{E}_{pilot}}{\hat{N}} \cdot \frac{E_b}{E_{pilot}}. \tag{3.13}$$

The feedback command for closed loop power control is then generated by comparing $\left(\frac{E_b}{N} \right)_{measured}$ against the threshold set by the outer loop.

3.3 LDPC Code Design

The design algorithm for the LDPC codes used is based on an idea from [24], which has been reported in [25]. Any parity check matrix H can be thought of as a many-to-many mapping from codeword bits to parity checks and vice versa. If we create a set $B = \{b_0, b_0, b_0, b_1, b_1, b_1, \cdots\}$ of the codeword bits b_i, with each bit b_i appearing in the set a number of times equal to the weight of that column of H, and a similar set $C = \{c_0, c_0, \cdots, c_1, c_1, \cdots\}$ of the parity checks, then any parity check matrix H corresponds to some one-to-one mapping (permutation) S from elements of B to elements of C. The goal is to find a mapping S that leads to a

suitable LDPC code matrix H. By "suitable" we mean that the resulting code has to have no 4-cycles. A 4-cycle occurs in the code if the bipartite graph defined by H has a path of length four that closes back on itself, i.e., there are bits b_i, b_j and checks c_k, c_l such that S takes an instance of b_i to c_k, S^{-1} takes an instance of c_k to b_j, S takes an instance of b_j to c_l, and S^{-1} takes an instance of c_l back to b_i. It has been found, both theoretically and empirically, that 4-cycles are detrimental to the error rate performance of LDPC codes.

The code design algorithm is as follows:

Step 1: Compute the desired codeword size N and number of parity checks M and randomly generate a permutation S of the desired size $N \times w_c$, where w_c is the column weight (the total number of ones in H).

Step 2: Check S to see that it corresponds to a valid H matrix. Not all permutations do; for example, a permutation that took one instance of b_0 to c_0 and another instance of b_0 to c_0 would not correspond to a valid H matrix; it would, in effect, be trying to put two ones in the same spot in H. We check the permutation for validity, and if we find any mappings in the permutation that lead to such problems, we randomly swap the target of that one mapping with some other mapping in S and repeat until we get a suitable S.

Step 3: Check the permutation for 4-cycles. If we find none, we proceed to *Step 6.*

Step 4: If we did find a 4-cycle involving some codeword bit b_i, we pick another codeword bit b_j and exchange the targets of the two checks that S maps these two bits to, and go back to Step 2. Ordinarily, we pick b_j by finding a bit in another cycle in S, in hopes of being able to destroy two cycles in S in one move. However, one time in every 50, we instead pick a b_j completely at random from among the N codeword bits. This is an ad hoc addition to the algorithm, which empirically helps keep the algorithm from failing to terminate.

Step 5: Now that we have done the exchange, go back to *Step 2*.

Step 6: Now we have an S corresponding to a cycle-free H matrix. The final stage is to ensure that H can be converted to a generator matrix G. The necessary and sufficient condition for this is that the rightmost $M \times M$ section of H be invertible. We check to see that this submatrix is invertible via Gaussian elimination. If the submatrix is invertible, we stop. If it is not, the Gaussian elimination will have stopped on a column, which is the source of the trouble; we simply exchange that column of H with another column and try again.

The above algorithm is admittedly rather ad hoc in nature. Whether the algorithm is likely to actually converge in any given situation is by no means certain. In practice, it appears that the algorithm converges much less rapidly as one attempts to create codes of rates much above 0.95, codes of very short length, and codes with column weight more than three.

3.4 Convolutional and Turbo Code Specifications

The specifications for convolutional codes and turbo codes come from [4]. For comparison purposes, the code rates we are considering are all ¼. For convolutional codes, the constraint length is nine and the generator functions are $g_0 = 765$ (octal), $g_1 = 671$ (octal), $g_2 = 513$ (octal), and $g_3 = 473$ (octal) respectively. At the end of each frame, eight encoder tail bits are used to set the state of the encoder registers to zero.

For turbo codes, the transfer function for the constituent code is

$$G(D) = \left[1 \quad \frac{n_0(D)}{d(D)} \quad \frac{n_1(D)}{d(D)}\right], \tag{3.14}$$

where $d(D) = 1 + D^2 + D^3$, $n_0(D) = 1 + D + D^3$, and $n_1(D) = 1 + D + D^2 + D^3$. Tail bits are inserted at the end of each frame to force the first constituent encoder to the zero state. The simulator uses a random interleaver instead of the standardized one specified in [4].

3.5 Simulation

Based on the fact that significant differences in coding gains can be found for different codeword sizes, we investigate the performance of systems with different coding techniques for various data rates, because the higher the data rate, the larger the codeword size for each 20 ms frame. We have generated LDPC

codes for four data rates respectively. The code rate is ¼ and the lengths of the codewords are varied from 1536 to 12288 bits. On AWGN channels, these LDPC codes perform remarkably well compared to convolutional codes when the codeword size is large. Fig. 3.2 shows E_b / N_o gains of LDPC over convolutional coding on AWGN channels. It is obvious that the longer the codeword, the better performance.

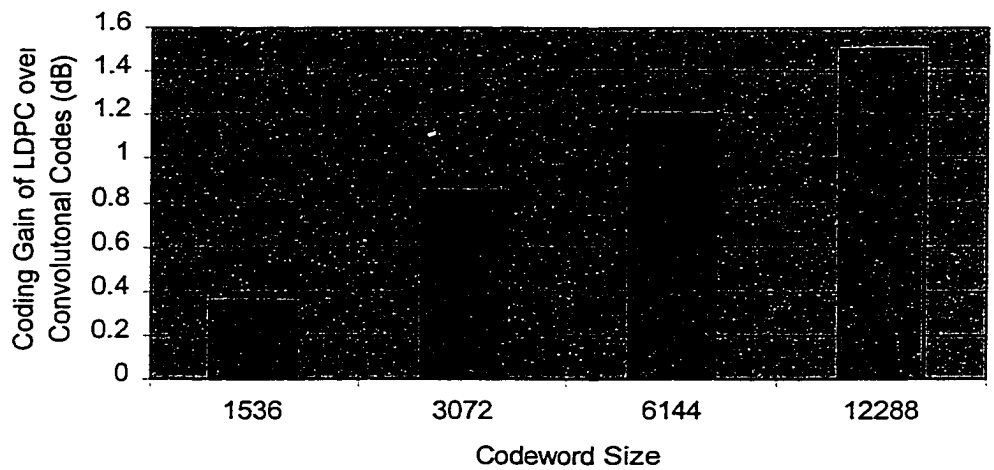


Fig. 3.2. Coding gain of LDPC over convolutional codes for AWGN channels.

In order to have a fair comparison, we use the same simulation parameters for all three coding techniques. However, the simulator used to compare the performance of LDPC and convolutional codes is a chip-level implementation, while the simulator used to compare turbo and convolutional codes is a symbol level implementation. The results are expected to be comparable. The simulation parameters are given in Table 3.2.

TABLE 3.2

SIMULATION PARAMETERS

Carrier frequency	2 GHz
Chip rate	1.2288 Mcps
Frame length	20 ms
Interleaver depth	20 ms (Block)
Code rate	1/4
Bit rate	9.6, 19.2, 38.4, 76.8 and 153.6 kb/s
PC puncturing	Included
Mobile location geometry	Ior/Ioc=8 dB
Pilot Ec/Ior	16.4% of the base station maximum transmission power
Max fraction power allocation	1.0 (relative to the base station maximum transmission power)
Min fraction power allocation	0.0 (relative to the base station maximum transmission power)
Inner-loop power control rate	800 Hz
Power control command error rate	4%
Inner-loop power control step up/down	+/-0.5 dB
Target Eb/No step	0.3 dB up (bad frame) and 0.0158 dB down (good frame)
Target frame error rate	5%
Frames per run	10,000 (plus 500 before starting to collect statistics)
Channel estimation window	1/12 of a power control group
Multipath channel	1-path Rayleigh fading
Maximum turbo decoder iterations	8

Since each user channel is spread with a different orthogonal code, the signals transmitted from the base station are orthogonal, and they do not mutually interfere in the absence of multipath. The other cell interference and thermal noise is approximated as Gaussian.

The soft data we fed into the Viterbi decoder are the demodulated and despread outputs of the receiver. However, both the LDPC and turbo decoders require an estimate of the SNR for every coded bit besides the despread output, which is approximated as Gaussian distributed. In our simulation, we assume this estimation to be perfect.

Table 3.3 shows our simulation results of the traffic power allocation of the system incorporating LDPC and convolutional coding techniques for various data rates and speeds of the vehicles.

When we consider a time-correlated Rayleigh fading channel, the channel changes faster when the vehicle is moving at a higher speed. We investigated three different speeds from low to high for the desired vehicle. When the fading is slow at 5 km/hr, the strength of the channel stays almost constant for many frames and the performance in this situation is similar to that of an AWGN channel. However, LDPC codes cannot perform as well as in AWGN channels, because when the signal is severely faded, it usually lasts for a long time, during which all symbols are simultaneously faded, resulting in very poor performance. However,

TABLE 3.3

TRAFFIC POWER ALLOCATIONS FOR IS-2000 FORWARD LINK INCORPORATING LDPC CODING AND CONVOLUTIONAL CODING TECHNIQUES

Speed (km/h)	9.6 kb/s CONV (dB)	19.2 kb/s CONV (dB)	19.2 kb/s LDPC (dB)	38.4 kb/s CONV (dB)	38.4 kb/s LDPC (dB)	76.8 kb/s CONV (dB)	76.8 kb/s LDPC (dB)	153.6 kb/s CONV (dB)	153.6 kb/s LDPC (dB)
5	-18.36	-15.39	-14.88	-12.16	-12.18	-8.90	-9.30	-5.71	-6.28
50	-21.79	-18.75	-18.33	-15.50	-15.58	-12.18	-12.69	-8.97	-9.63
100	-22.62	-19.50	-19.23	-16.14	-16.43	-12.92	-13.50	-9.63	-10.54

the situation is not so serious for the fading at 100 km/hr, because for such high speed, the fading is very fast. Even if there is a deep fade at one moment, it will not last long. Fig. 3.3 shows the corresponding average transmitted power gain of LDPC over convolutional coding for the IS-2000 forward link. Where the required power is larger for LDPC codes than for convolutional codes, the gain is negative. We can see from the figure that when the data rate is 19.2 kb/s or lower, the LDPC code is 0.51 dB worse than the convolutional code at 5 km/hr and 0.27 dB worse at 100 km/hr. When the data rate is higher, the performance of LDPC codes gets better. At 153.6 kb/s, LDPC codes outperform convolutional codes by 0.57 dB at 5 km/hr and 0.91 dB at 100 km/hr.

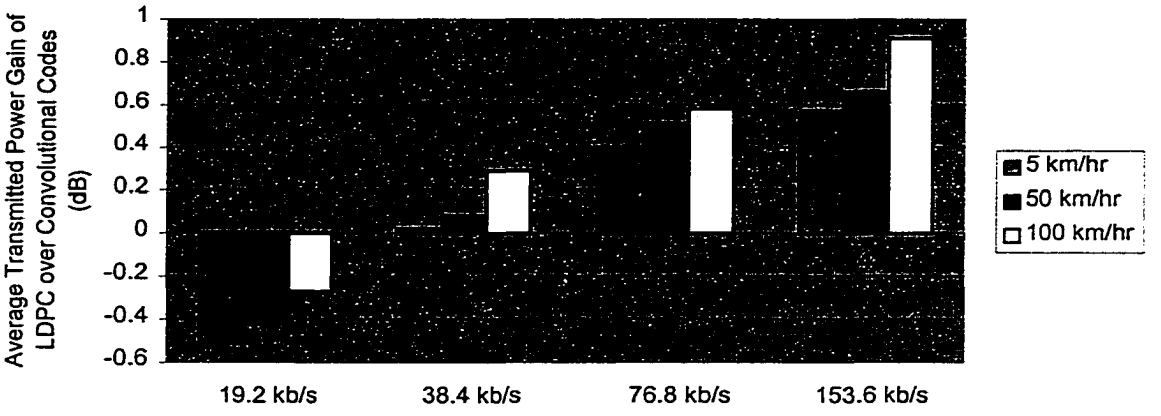


Fig. 3.3. Average transmitted power gain of LDPC over convolutional coding for the IS-2000 forward link.

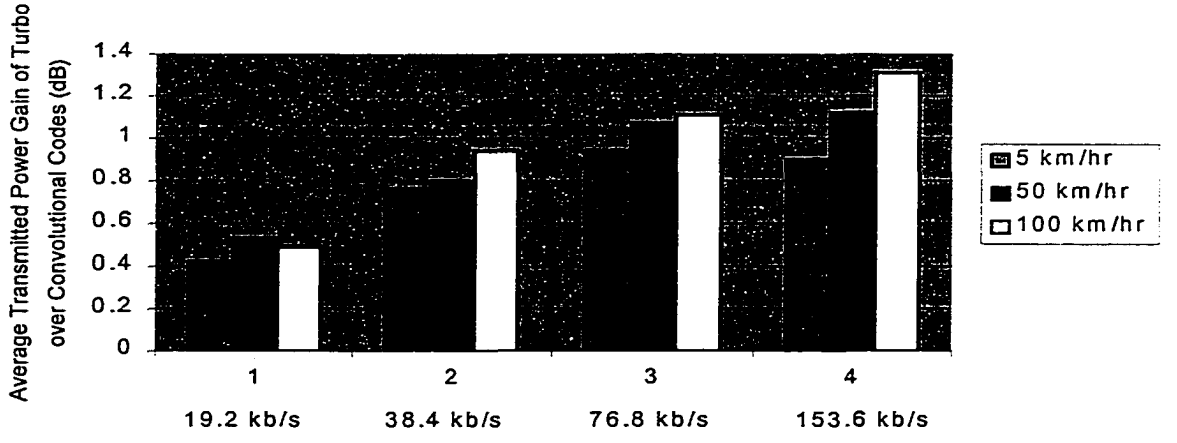


Fig. 3.4. Average transmitted power gain of turbo over convolutional coding for the IS-2000 forward link.

Compared with LDPC coding, turbo codes perform even better. Fig. 3.4 shows the average transmitted power gain of turbo over convolutional codes for the IS-2000 forward link. At 19.6 kb/s, turbo codes outperform LDPC coding by approximately 0.76~0.95 dB. As the data rate increases, the performance of LDPC codes improves a bit faster. At 153.6 kb/s, the difference in performance between LDPC and turbo coding has decreased to 0.33~0.46 dB.

3.6 Decoding Complexity and Memory Requirement

We investigate the computational complexity of LDPC decoding using the results given in [26]. Table 3.4 summarizes these results in terms of operations per information bit per iteration, where I is the number of states of the constituent convolutional code, J is their constraint length, R is the code rate and w_c is the column weight.

TABLE 3.4

COMPARISON OF COMPLEXITY OF TURBO AND LDPC DECODING

	Additions	Look-ups	Compares
LDPC decoding	$(4w_c - 1)/R$	$4w_c / R$	0
Forward and backward algorithm for convolutional code	$14I$	$4I$	$4I$

For the specifications used in our simulation, we show a comparison in decoding complexity for the LDPC and turbo codes in Table 3.5.

TABLE 3.5

COMPARISON OF COMPLEXITY OF TURBO AND LDPC DECODING

	Additions	Look-ups	Compares
LDPC decoding $w_c = 3, R = 1/4$	44	48	0
Turbo decoding with two 8-state codes	224	64	64

From Table 3.5, we can see that the number of operations required for LDPC decoding is much smaller than turbo decoding with a pair of 8-state constituent codes which we have used for the simulation. It is also shown in [27] that a pair of 4-state concatenated decoders performing eight iterations imposes the same load as a $J = 9$ Viterbi decoder, which we have used for the convolutional codes in our simulation.

As for the memory requirement of the LDPC, turbo and convolutional decoding, the forward and backward algorithm only needs to store $2L$ sets of state metrics, where L is the number of branches for the "learning" period of the algorithm, which should be greater than five times the constraint length J of the code. If we assume that the code uses 32-bit state metrics, then for the convolutional code we used in our simulation with constraint length of nine, the required memory should

be $256*32*5*J*2/8=90\,KB$. For the turbo code we have used in our simulation, because the component code constraint length is shorter $(J=4)$, the required memory should be $2.5\,KB$. For the LDPC code, we need to store the parity check matrix. The bigger the codeword size, the larger the memory needed. We have used in our simulation four different LDPC codes with codeword sizes 1536, 3072, 6144 and 12288 corresponding to four different data rates. The column weight of these codes was three. Assuming sixteen bits are required to represent each row or column index, the memory that is required to store the parity check matrix is 18, 36, 72 and 144 KB respectively. Compared with turbo decoding, LDPC decoding requires much more memory.

3.7 Theoretical Noisy Channel Estimates

In the previous simulation of coding techniques, we assume the despread outputs are approximated as Gaussian distributed and the SNR for each code symbol is perfectly known. However, we consider channel estimation in our simulations, so the resulted channel estimates are not perfect. How does the imperfection influence the final performance results?

For simplicity of analysis, if we assume the instantaneous received signal for the current chip period i is

$$y_i = \beta\, s + n_1(i), \tag{3.15}$$

where

$$\beta = \alpha\, e^{j\theta}, \quad s = \sqrt{P_t} e^{j\phi},$$

are channel fading and transmitted symbols respectively. The variance of the multiple access interference n_1, which is approximated as a Gaussian process, has variance $2\sigma_{n_1}^2$ and the Rayleigh variable β has $E[\beta^2] = 2\sigma_\beta^2$. Also, we assume the estimated channel parameter is expressed as

$$h = \beta + n_2, \tag{3.16}$$

where n_2 is the estimation noise with variance $2\sigma_{n_2}^2$. The pdf of h is expressed as [28]

$$p_H(h) = \frac{1}{2\pi\sigma_h^2} exp[\frac{|h|^2}{2\sigma_h^2}]. \tag{3.17}$$

We have the following relationship

$$2\sigma_{n_2}^2 = 2M\sigma_{n_1}^2 / (2 \cdot M \cdot \sqrt{P_p})^2, \tag{3.18}$$

according to (3.5)-(3.9).

Then the decision variable for each chip is

$$z_i = y_i h^*, \tag{3.19}$$

and the despread decision variable for each symbol is

$$U = \sum_{i=1}^{M} z_i = U_{real} + jU_{imag}. \tag{3.20}$$

We define the cross-correlation coefficient of y_i and h_i as

$$\rho = \frac{E[y_i h_i^*]}{\sqrt{E[|y_i|^2]E[|h_i|^2]}} = \frac{\sqrt{P_t} e^{j\phi} \cdot 2\sigma_\beta^2}{\sqrt{(P_t 2\sigma_\beta^2 + 2\sigma_{n_1}^2)(2\sigma_\beta^2 + 2\sigma_{n_2}^2)}} = |\rho| e^{j\phi}. \tag{3.21}$$

According to Frenger's derivation in [28], the variable z_i conditional on H and s is complex valued Gaussian distributed with mean $\rho|h|^2\frac{\sigma_y}{\sigma_h}$ and variance $2\sigma_y^2(1-|\rho|^2)|h|^2$, then the pdf of the sum of these Gaussian random variables U can be evaluated as

$$p_{U\backslash s}(u)=\int_{R_H}p_{U,H\backslash s}(u,h)=\int_{R_H}p_{U\backslash H,s}(u)p_H$$

$$=\int_{R_H}\frac{1}{(2\pi)^2\sigma_h^2\sigma_y^2(1-|\rho|^2)|h|^2M}exp[-\frac{\left|u-M\rho|h|^2\frac{\sigma_y}{\sigma_h}\right|^2}{2\sigma_y^2(1-|\rho|^2)|h|^2M}-\frac{|h|^2}{2\sigma_h^2}], \qquad (3.22)$$

where the region of integration R_H is the entire complex plane.

Using transformation of variables, we can evaluate (3.22) as

$$p_{U\backslash s}(u)=$$

$$\frac{1}{2\pi\sigma_h^2\sigma_y^2(1-|\rho|^2)M}exp(\frac{\Re(u\rho^*)}{\sigma_y\sigma_h(1-|\rho|^2)})K_0(\frac{|u|\sqrt{(M-1)|\rho|^2+1}}{\sigma_y\sigma_h(1-|\rho|^2)\sqrt{M}}), \qquad (3.23)$$

where $K_0[]$ is the modified bessel function of the second kind with order 0.

Expression (3.23) can be further written as

$$p_{U\backslash s}(u_{real},u_{imag})$$

$$=\frac{1}{2\pi\sigma_h^2\sigma_y^2(1-|\rho|^2)M}exp(\frac{|\rho|(u_{real}cos\phi+u_{imag}sin\phi)}{\sigma_y\sigma_h(1-|\rho|^2)})K_0(\frac{|u|\sqrt{(M-1)|\rho|^2+1}}{\sigma_y\sigma_h(1-|\rho|^2)\sqrt{M}}). \qquad (3.24)$$

The following transformation of random variables

$$r = \sqrt{u_{real}^2 + u_{imag}^2}, \quad \theta = tan^{-1}(\frac{u_{imag}}{u_{real}}), \tag{3.25}$$

yields the joint pdf of the envelop r and θ in the form

$$p_{U\backslash s}(r,\theta)$$
$$= \frac{r}{2\pi\sigma_h^2\sigma_y^2(1-|\rho|^2)M} exp(\frac{|\rho| r cos(\theta-\phi)}{\sigma_y\sigma_h(1-|\rho|^2)}) K_0(\frac{r\sqrt{(M-1)|\rho|^2+1}}{\sigma_y\sigma_h(1-|\rho|^2)\sqrt{M}}). \tag{3.26}$$

Then integration over the variable r yields the marginal pdf of the phase θ, according to which we will get the reliability information for each coded symbol, because we used QPSK modulation. We have

$$p(\theta) = \frac{c_3}{c_2^2}[hypergeom([1,1],[1/2], \frac{c_1^2 cos^2(\theta-\phi)}{c_2^2})$$
$$+ \frac{\pi^3 c_1 cos(\theta-\phi)}{2c_2} hypergeom([3/2],[\ ], \frac{c_1^2 cos^2(\theta-\phi)}{c_2^2})], \tag{3.27}$$

where

$$c_1 = \frac{|\rho|}{\sigma_y\sigma_h(1-|\rho|^2)},$$
$$c_2 = \frac{\sqrt{(M-1)|\rho|^2+1}}{\sigma_y\sigma_h(1-|\rho|^2)\sqrt{M}},$$
$$c_3 = \frac{1}{2\pi\sigma_h^2\sigma_y^2(1-|\rho|^2)M},$$

and *hypergeom*(•) is Gauss' hypergeometric functions with

$$hypergeom([3/2],[\ ], z) = \frac{1}{(1-z)^{\frac{3}{2}}}.$$

We can see from (3.27) that considering imperfect channel estimation results in a very complicated calculation for the reliability of the code symbols. Fortunately,

for the forward link of IS-2000 system, using pilot channel and a moving average filter, the channel estimation is relatively accurate, so usually we do not have to worry about the imperfect channel estimation on the reliability calculation of code symbols.

3.8 Conclusions

In this chapter, we investigated the performance of different coding strategies for the forward link of an IS-2000 system over time-correlated Rayleigh fading channels for various data rates and vehicle speeds. Our results showed that when the data rate is 9.6 kb/s or lower, the convolutional code with a constraint length of nine outperforms both turbo and LDPC coding. At 19.2 kb/s, the turbo code already outperforms the convolutional code. When the data rate is even higher, that means for each 20 ms frame, the codeword size is larger than 3072 bits, the LDPC codes we have designed show their advantage over convolutional codes, however its performance is not as good as turbo codes. The LDPC codes used in the simulation are regular LDPC codes (which have a parity-check matrix with a uniform number of non-zero entries in each column or row). It has been shown that properly designed irregular LDPC codes (with parity check matrices that have varying numbers of non-zero entries in each column and row) can perform better than turbo codes and extremely close to the theoretical limits [24]. Furthermore, LDPC decoding requires many fewer operations than turbo decoding. In addition, it is possible for LDPC codes to use the parity checks to

detect when a valid codeword has been found so that unnecessary iterations are avoided and the average number of iterations is reduced [26]. One of the major disadvantages of LDPC decoding is its large memory requirement.

Chapter 4

Interference Analysis of CDMA Systems

4.1 Introduction

Several users can transmit messages simultaneously over the same radio bandwidth in CDMA systems. Each of the users uses a specific PN code. For the forward link of CDMA cellular systems, the desired user receives interference from other base stations around it besides the desired signal transmitted by its own base station. The maximum number of users that can be supported by a CDMA cellular system is mainly limited by the multiple access interference effects.

In link level simulation of CDMA systems, the multiple access interference is usually modeled as a Gaussian process, whose variance is determined by an input parameter, the mobile location geometry. If we are going to consider a multicell environment, the computation work for link level simulation is exorbitant. In order to study the interference from a multicell environment point of view, we

need to construct a comprehensive model for the BER analysis of the forward link of CDMA systems.

Propagation of continuous waves with a very high frequency in CDMA cellular radio systems is largely influenced by three typical propagation phenomena: path loss, multipath fading and shadowing [29]. Multipath fading is usually called fast fading and modeled as a Rayleigh distribution, which is added to the log-normal shadowing effect. Shadowing has an effect on the received local-mean signal power of the users. Usually, it is influenced by natural and man-made obstructions. So if the desired and interfering signal experience the same obstacles, they are correlated to each other. The presence of correlated shadowing is most obvious for the forward link [30]. It is considered to be a more realistic model for capacity analysis, especially for the indoor environment.

Although many research results have been published on the link level BER analysis of CDMA systems [31] - [33], there are only a few which address the effect of interferers in a multicell DS-CDMA environment inclusive of the mobiles' spatial location. For the purpose of accurate capacity analysis, we need to consider the overall situation. The Gaussian approximation, which is usually used for the performance analysis of the system, leads to complicated expressions due to the need to account for the mobiles' spatial location, fast fading, and shadowing effects with increasing number of interfering cells.

The authors in [34] considered the exact location of the desired mobile and derived a simplified expression for BER analysis over Rayleigh fading channels for both the forward and reverse link. In [35], the authors generalized the results of [34] to Nakagami fading. They derived a closed form conditional probability density function of the Nakagami-faded-interference-to-signal power ratio, which is used to compute the BER of the forward link of a DS-CDMA system. As far as we know, these two papers are the first to use a simplified version of BER analysis, which includes both the spatial locations of the desired user and multipath fading effects in a multicell environment. However, the log-normal shadowing effect papers for the forward link of CDMA systems is ignored in these papers.

We use two different models to characterize the shadowing effect of the system. The first model comes from [36]. In this book, Viterbi expresses the random component of the decibel loss as the sum of two components. One is in the near field of the desired user, which is assumed to be only influenced by the user and common to all the base stations around. The other is only related to one and only one specific base station and independent from one base station to another. Thus in this model, the signal received by the desired mobile is correlated to all the interfering signals coming from the other base stations around.

The other model comes from [37]. Because in our situation, we are only considering the instantaneous SIR, which is going to influence the momentary

BER of the system, we ignore the autocorrelation and only concern ourselves with the crosscorrelation effect of the log-normal shadowing of the cellular system. Based on experimental data, Mawira pointed out in [37] that the main factor affecting the value of the normalized crosscorrelation coefficient is the angle θ between the "rays" from the mobile station to the two base stations. Analysis of the experimental data shows that the normalized crosscorrelation coefficient rapidly decreases with increasing value of the angle θ.

We will consider the BER of the desired mobile with random location in the cell and study how the correlation of the log-normal shadowing is going to influence the overall performance of the system in a multicell environment. The combined probability density function approach introduced in [34] and [35] will greatly reduce the complexity of the computation.

4.2 Analytical Model

Fig. 4.1 is a DS-CDMA cellular system with nineteen unit length hexagonal cells. We use a two-layer structure around the central cell to capture the multiple access interference effects of surrounding cells. We assume the base stations are located at the centers of the cells, and the base station in each cell serves K active mobile users, which are uniformly distributed in the cell. Power control is used to compensate for the path loss and log-normal shadowing associated with each signal received at the base station. The signal is assumed to experience Rayleigh

fading on top of the log-normal shadowing.

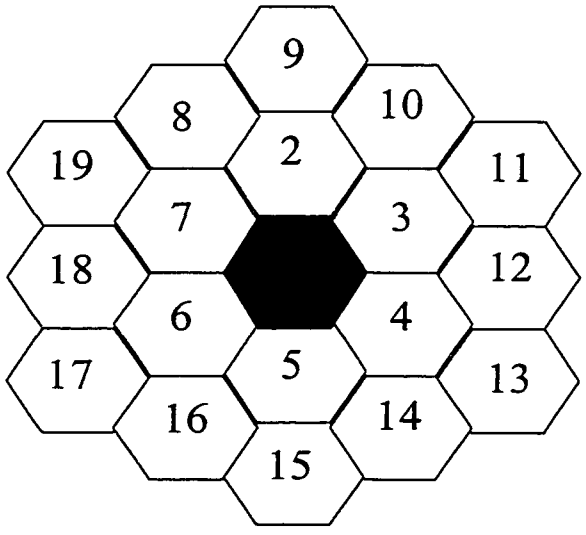


Fig. 4.1. Hexagonal cell configuration.

For a user at a distance d from a base station, attenuation is proportional to [36]

$$\beta(d,\delta) = d^{\lambda} 10^{\frac{\delta}{10}}, \tag{4.1}$$

where δ is the decibel attenuation due to shadowing with zero mean and standard deviation σ_δ and λ is the path loss exponent. Experimental data suggests that $\lambda = 4$ and $\sigma_\delta = 8\,dB$ are typical values for these parameters [7].

We assume that all the users have the same average received signal power as a result of a perfect power control strategy and the power control cannot track the fast fading. Because the CDMA system is multiple access interference limited, we ignore the background thermal noise here for simplicity of analysis. Thus the

received signal at the tagged mobile of cell 1 with average power control energy $2P$ is:

$$r(t) = \sum_{n=1}^{N} \frac{\alpha_n (d_{11}^{\lambda} 10^{\frac{\delta_{1,1}}{10}})^{\frac{1}{2}}}{(d_{n1}^{\lambda} 10^{\frac{\delta_{n,1}}{10}})^{\frac{1}{2}}} \sum_{i=(n-1)K+1}^{nK} \sqrt{2P}\, b_i(t-\tau_i)\, W_i(t-\tau_i)\, PN_i(t-\tau_i) \cos(\omega_c t + \theta_i), \quad (4.2)$$

where

i - ith mobile,

$n-nth$ base station,

$\sqrt{2P}$ - unfaded amplitude of the received signal at the mobile stations,

ω_c - angular carrier frequency,

$b_i(t)$ - random binary information data waveform which takes the value ± 1,

$W_i(t)$ - binary Walsh code waveform which takes the value ± 1,

$PN_i(t)$ - pseudonoise spreading waveform which takes the value ± 1,

τ_i - time delay uniformly distributed over $[0, T_b]$,

T_b - information bit duration,

θ_i - phase delay uniformly distributed over $[0, 2\pi]$,

d_{ni} - distance from the base station in cell n to the ith mobile.

The independent fast-fading random variable α_n's are assumed constant over at least one symbol duration. For our analysis, they are taken to follow Rayleigh distributions.

For simplification of analysis, we consider BPSK modulation. It is well known that the output of the correlation receiver at each sampling time can be written as [32]

$$U = \int_{\tau_1}^{T_b+\tau_1} r(t)\, c_1(t-\tau_1)\alpha_1 \cos(\omega_c t+\theta_1)dt$$
$$= S + I_{ma}, \tag{4.3}$$

where

$$c_i(t) = W_i(t)\, PN_i(t),$$

$$S = \sqrt{\frac{P}{2}}\, b_0 T_b \alpha_1^2,$$

$$I_{ma} = \sqrt{\frac{P}{2}}\alpha_1^2 \sum_{i=2}^{K}\left\{b_{-1}^i R_{i,1} + b_0^i \hat{R}_{i,1}\right\}\cdot(\tau_i - \tau_1)\cos(\theta_i - \theta_1) +$$

$$\sqrt{\frac{P}{2}}\sum_{n=2}^{N}\frac{\alpha_1\alpha_n (d_{11}^{\lambda} 10^{\frac{\delta_{1,1}}{10}})^{\frac{1}{2}}}{(d_{n1}^{\lambda} 10^{\frac{\delta_{n,1}}{10}})^{\frac{1}{2}}}\sum_{i=(n-1)K+1}^{nK}\left\{b_{-1}^i R_{i,1} + b_0^i \hat{R}_{i,1}\right\}\cdot(\tau_i - \tau_1)\cdot\cos(\theta_i - \theta_1),$$

here

$$R_{i,1}(\tau) = \int_0^{\tau} c_i(t-\tau)\, c_1(t)\, dt,$$
$$\hat{R}_{i,1}(\tau) = \int_{\tau}^{T_b} c_i(t-\tau)\, c_1(t)\, dt,$$

and

b_0^i is the information bit to be detected for the *ith* user, b_1^i is the preceding bit for the *ith* user. Please note that we include the spatial location of the user and shadowing effect in the whole derivation process.

It is assumed that the mobile radio system has a sufficiently large processing gain (128 in our situation) and serves a sufficient number of users for the instantaneous

composite interference at a mobile receiver to be Gaussian distributed. If we use Gaussian approximation, because the variance of I_{ma} can be approximated as

$$\sigma_{ma}^2 \approx \frac{PT_b^2}{6M}\{(K-1)\alpha_1^4 + \sum_{n=2}^{N} \frac{K\alpha_1^2\alpha_n^2 d_{11}^{\lambda} 10^{\frac{\delta_{1,1}}{10}}}{d_{n1}^{\lambda} 10^{\frac{\delta_{n,1}}{10}}}\}, \tag{4.4}$$

where M is the processing gain, the instantaneous SIR conditioned on α_n's and δ_{1n}'s at the receiver of the desired mobile is

$$SIR = \frac{S^2}{\sigma_{ma}^2} = \frac{3M}{(K-1) + \sum_{n=2}^{N} K(d_{11}/d_{n1})^{\lambda}(\alpha_n^2/\alpha_1^2)10^{\frac{\delta_{1,1}-\delta_{n,1}}{10}}}. \tag{4.5}$$

Based on the instantaneous SIR and the assumption that the fast fading α_i's are independent from one base station to another, the unconditional probability of error at a mobile user located at Cartesian coordinates (x, y) with the origin located at the base station of the central cell for an N-cell configuration is given by

$$P_e(x,y) = \int_0^{\infty} d\alpha_1 \cdots \int_0^{\infty} d\alpha_N \int_{-\infty}^{+\infty} d\delta_{1,1} \cdots \int_{-\infty}^{+\infty} d\delta_{N,1}\ p(\alpha_1)\cdots p(\alpha_N) pdf_{\delta_{1,1},\cdots,\delta_{N,1}}(\delta_{1,1},\cdots,\delta_{N,1})$$
$$\cdot Q\left(\left[\frac{(K-1) + \sum_{n=2}^{N} K(d_{11}/d_{n1})^{\lambda}(\alpha_n^2/\alpha_1^2)10^{\frac{\delta_{1,1}-\delta_{n,1}}{10}}}{3M}\right]^{-1/2}\right). \tag{4.6}$$

If we use Gauss' formula, we can get the numerical integration value of BER. But when N is large, the truncation error and computation time become unacceptable. Here we use a simplified version of the BER expression to do numerical evaluation.

4.3 Extended Combined PDF Approach [34]

Let us look at how we can get the probability density function of the following variable:

$$W = \sum_{n=2}^{N} (d_{11}/d_{n1})^{\lambda} 10^{\frac{\delta_{1,1}-\delta_{n,1}}{10}} (\alpha_n^2/\alpha_1^2) = \sum_{n=2}^{N} f_n(d,\delta)(\alpha_n^2/\alpha_1^2), \tag{4.7}$$

where

$f_n(d,\delta) = (d_{11}/d_{n1})^{\lambda} 10^{\frac{\delta_{1,1}-\delta_{n,1}}{10}}$ and α_n is a Rayleigh distributed random variable with pdf

$$pdf_{\alpha_n}(\alpha_n) = \frac{2\alpha_n}{\overline{\alpha_n^2}} exp(-\frac{\alpha_n^2}{\overline{\alpha_n^2}}), \tag{4.8}$$

where $\overline{\alpha_n^2}$ is the mean square value of α_n, which depends on the path loss and log-normal shadowing.

Through variable transformations $\beta_n = f_n(d,\delta)\alpha_n^2$ and $L_n = f_n(d,\delta)\overline{\alpha_n^2}$, we can get

$$pdf_{\beta_n}(\beta_n) = \frac{1}{L_n} exp(-\frac{\beta_n}{L_n}). \tag{4.9}$$

The derivation of the pdf of W is performed in two steps. First the pdf of the variable

$$W' = \sum_{n=2}^{N} f_n(d,\delta)\alpha_n^2 = \sum_{n=2}^{N} \beta_n \tag{4.10}$$

is evaluated. Because the Laplace transform of the sum of the variables is equal to the product of the Laplace transforms of each variable, we first have the Laplace transform of W' as

$$\psi(W') = \prod_{n=2}^{N} \frac{\frac{1}{L_n}}{s + \frac{1}{L_n}}. \tag{4.11}$$

Taking the inverse transform of (4.11), we have the pdf of W' as

$$pdf_{W'}(W') = \sum_{n=2}^{N} \frac{e^{-\frac{W'}{L_n}}}{L_n} \prod_{\substack{i=2 \\ i \neq n}}^{N} \frac{1}{1 - \frac{L_i}{L_n}}. \tag{4.12}$$

The pdf of W is obtained by evaluating the pdf of $\frac{W'}{\alpha_1^2}$ using the convolution of the pdf's of W' and α_1^2 [38]. So the pdf of W conditioned on a fixed location of the vehicle and the log-normal shadowing parameters is derived as follows

$$pdf_W(W) = \sum_{n=2}^{N} \left[\frac{(W + \frac{L_n}{L_1})^2}{\frac{L_n}{L_1}} \prod_{\substack{i=2 \\ i \neq n}}^{N} (1 - \frac{L_i}{L_n}) \right]^{-1}$$

$$= \sum_{n=2}^{N} \left[\frac{(W + f_n(d,\delta))^2}{f_n(d,\delta)} \prod_{\substack{i=2 \\ i \neq n}}^{N} (1 - \frac{f_i(d,\delta)}{f_n(d,\delta)}) \right]^{-1}. \tag{4.13}$$

This expression is a more general and corrected version of a result given in [39]. Thus the probability of error for a fixed vehicle location given the instantaneous SIR can be simplified to

$$P_e(x,y) = \int_0^\infty dW \int_{-\infty}^{\infty} d\delta_{1,1} \cdots \int_{-\infty}^{\infty} d\delta_{N,1} \; pdf_W(W) pdf_{\delta_{1,1},\cdots,\delta_{N,1}}(\delta_{1,1},\cdots,\delta_{N,1}) \cdot Q\left(\left[\frac{(K-1)+KW}{3M}\right]^{-1/2}\right). \tag{4.14}$$

4.4 Shadowing Environment

There are several ways to deal with the joint pdf of $\delta_{n,1}$'s.

4.4.1. Pure Fading

If we just consider the path loss due to the location of the desired user and the fast fading of the signals, the BER at the receiver of the user based on the instantaneous SIR without considering the shadowing effect is

$$P_e(x,y) = \int_0^\infty pdf_W(W) \cdot Q\left(\left[\frac{(K-1)+KW}{3M}\right]^{-1/2}\right) dW, \tag{4.15}$$

where

$$pdf_W(W) = \sum_{n=2}^{N}\left[\frac{(W+f_n(d,\delta))^2}{f_n(d,\delta)} \prod_{\substack{i=2 \\ i\neq n}}^{N} (1-\frac{f_i(d,\delta)}{f_n(d,\delta)})\right]^{-1},$$

and

$f_n(d,\delta) = f_n(d) = (d_{11}/d_{n1})^{\lambda}$.

Notice from (4.15), the number of integrals does not depend on the number of interfering cells in the system. This is the situation considered in [34].

For example, if we choose (0.5,0.5) as the physical location of the desired user in cell 1, the performance in terms of BER for 19-cell and 7-cell configurations with different number of users is shown in Fig. 4.2.

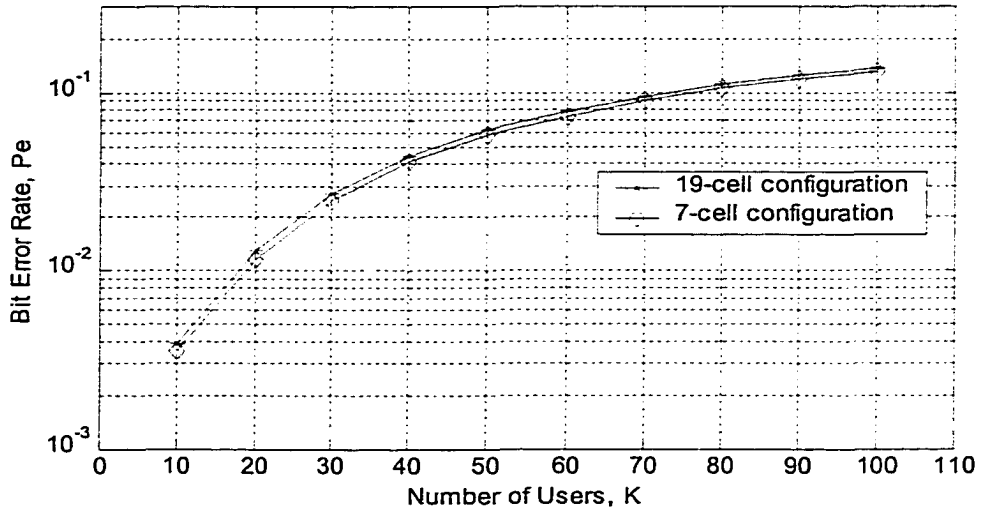


Fig. 4.2. Performance of 19-cell and 7-cell configuration at location (0.5, 0.5) for the forward link with different number of users.

We can see from Fig. 4.2 that the difference in BER between the two-layer structure (19-cell configuration) and the one-layer structure (7-cell configuration) is between 0.0005~0.005, which is small compared with a BER of 0.0039~0.137. The reason for this is that in the second layer of cells around the cell with the desired user, the path loss is relatively larger than in the cells for the first layer, so they have little effect on the performance of the system. Although in this situation, there is no difference between the computational complexity of the 19-cell and 7-cell configuration, it will influence the computational complexity if the number of integrals we use for the BER analysis increases with the number of

interfering cells, which is the situation in the following analysis. So in the following, we take a 7-cell configuration for simplicity of computation.

4.4.2. Viterbi's Log-normal Shadowing Model

Viterbi expresses the random component of the decibel path loss $\delta_{n,1}$ as the sum of two components [36]

$$\delta_{n,1} = a\delta + b\Delta\delta_{n,1}, \tag{4.16}$$

where

$a^2 + b^2 = 1, \quad a \le 1,$

with

$E(\delta_{n,1}) = E(\delta) = E(\Delta\delta_{n,1}) = 0,$
$Var(\delta_{n,1}) = Var(\delta) = Var(\Delta\delta_{n,1}) = \sigma_\delta^{\,2},$
$E(\Delta\delta_{i,1}\Delta\delta_{j,1}) = 0, \qquad for\ all\ i \neq j,$
$E(\delta_{i,1}, \delta_{j,1}) / \sigma_\delta^{\,2} = a^2 = 1 - b^2.$

The term $a\delta$ represents the part in the near field of the desired user which is common to all the base stations around, $b\Delta\delta_{n,1}$ is the part which is only related to the base stations and is independent from one base station to another. If we define

$$\omega_n = \delta_{1,1} - \delta_{n,1} = b(\Delta\delta_{1,1} - \Delta\delta_{n,1}), \tag{4.17}$$

then

$$\begin{aligned} E(\omega_n) &= 0, \\ Var(\omega_n) &= 2b^2\sigma_\delta^2, \end{aligned} \tag{4.18}$$

where ω_i and ω_j are independent from each other for $i \neq j$.

Thus the instantaneous SIR conditioned on the α_n's and ω_n's at the receiver of the tagged mobile is

$$SIR = \frac{S^2}{\sigma_{ma}^2} = \frac{3M}{(K-1) + \sum_{n=2}^{N} K(d_{11}/d_{n1})^{\lambda}(\alpha_n^2/\alpha_1^2)10^{\frac{\omega_n}{10}}}. \quad (4.19)$$

Based on the instantaneous SIR and the assumption that the fast fading α_i's and ω_n's are independent from one base station to another base station, the unconditional probability of error for a fixed vehicle location (x, y) for an N-cell configuration is given by [36]

$$P_e(x,y) = \int_0^{\infty} dW \int_{-\infty}^{+\infty} d\omega_2 \cdots \int_{-\infty}^{+\infty} d\omega_N \; Q\left(\left[\frac{(K-1)+KW}{3M}\right]^{-1/2}\right) pdf_W(W)\, pdf_{\omega_2 \cdots \omega_N}(\omega_2, \cdots, \omega_N), \quad (4.20)$$

where

$$pdf_W(W) = \sum_{n=2}^{N}\left[\frac{(W + f_n(d,\delta))^2}{f_n(d,\delta)} \prod_{\substack{i=2 \\ i\neq n}}^{N}\left(1 - \frac{f_i(d,\delta)}{f_n(d,\delta)}\right)\right]^{-1},$$

$$f_n(d,\delta) = (d_{11}/d_{n1})^{\lambda} 10^{\frac{\omega_n}{10}},$$

$$pdf_{\omega_2 \cdots \omega_N}(\omega_2, \cdots, \omega_N) = \frac{1}{(\sqrt{2\pi})^{N-1}(\sqrt{2}b\sigma_{\delta})^{N-1}} exp\left(-\frac{\omega_2^2 + \omega_3^2 + \cdots + \omega_N^2}{4b^2\sigma_{\delta}^2}\right).$$

The parameter b reflects some correlation between "rays" from the user to two base stations, that means if the standard deviation of the log-normal shadowing is fixed, the larger b is, the smaller is a, so is the common part for all base stations, which expresses the correlation between "rays". Fig. 4.3 shows the BER performance for $b^2 = 0.25, 0.5$ and 1.0 respectively.

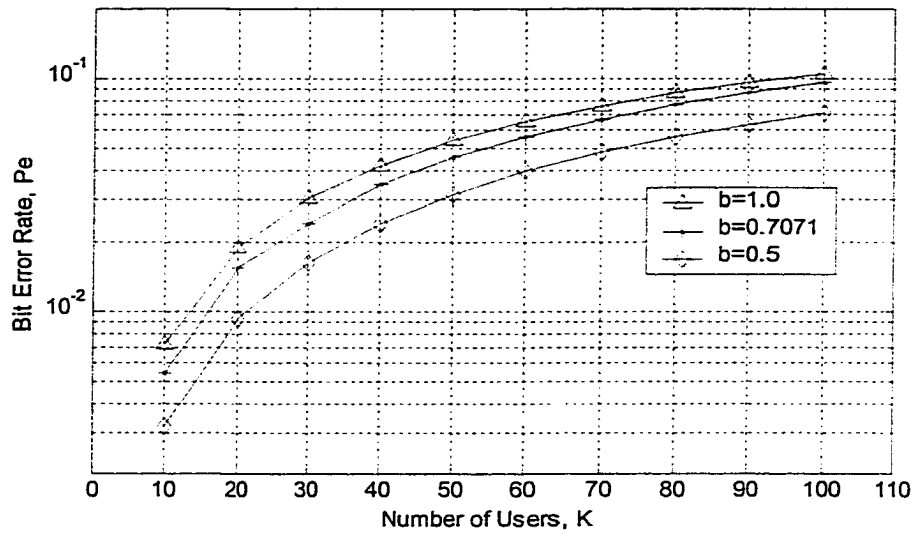


Fig. 4.3. Performance of a 7-cell configuration at location (0.5, 0.5) for the forward link with different number of users and b as a parameter.

We can see from Fig. 4.3 that when the correlation between the signals and interferences is large, which is expressed by smaller b 's, the performance of the system is better. Usually, correlated shadowing occurs when desired and interfering signals have very similar propagation paths, *i.e.*, encounter the same shadowing obstacles [29]. Compared with a pure fading situation, the difference in BER can be as large as 0.05 (for $b = 0.5$), which cannot be ignored in the real situation.

4.4.3. Mawira's Shadowing Model

In the real situation, the shadowing of signals and interferences received by a mobile station are correlated. It is concluded in [37] that the main factor affecting the value of the normalized crosscorrelation coefficient between the shadowing of signal and interference is the angle between the 'rays' from the mobile station to the two base stations. If we assume that the crosscorrelation coefficient between the signals received from the base station in cell i and in cell j is ρ_{ij} and the variance of δ_{1i} is σ_{1i}, then based on the instantaneous SIR, the unconditional probability of error for a random vehicle location (x, y) for an N-cell configuration is given by [40]

$$P_e(x,y) = \int_0^\infty dW \int_{-\infty}^{+\infty} d\delta_{1,1} \cdots \int_{-\infty}^{+\infty} d\delta_{N,1} \int_0^\infty Q\left(\left[\frac{(K-1)+KW}{3M}\right]^{-1/2}\right) pdf_W(W)\, pdf_{\delta_{1,1},\cdots,\delta_{N,1}}(\delta_{1,1},\cdots,\delta_{N,1}), \qquad (4.21)$$

where

$$pdf_W(W) = \sum_{n=2}^{N}\left[\frac{(W+f_n(d,\delta))^2}{f_n(d,\delta)} \prod_{\substack{i=2 \\ i\neq n}}^{N}\left(1-\frac{f_i(d,\delta)}{f_n(d,\delta)}\right)\right]^{-1},$$

$$f_n(d,\delta) = \frac{d_{11}^{\lambda} 10^{\frac{\delta_{1,1}}{10}}}{d_{n1}^{\lambda} 10^{\frac{\delta_{n,1}}{10}}},$$

$$pdf_{\delta_{1,1},\cdots,\delta_{N,1}}(\delta_{1,1},\cdots,\delta_{N,1}) = \frac{1}{(2\pi)^{\frac{N}{2}} |\Omega_X|^{\frac{1}{2}}} exp[-\frac{1}{2} X_\delta^T \Omega_X^{-1} X_\delta],$$

and

$$X_\delta = (\delta_{1,1}, \cdots, \delta_{N,1})^T,$$

$$\Omega_X = \begin{bmatrix} \sigma_1^2 & \mu_{12} & \mu_{13} & \cdots & \mu_{1N} \\ \mu_{21} & \sigma_2^2 & \mu_{12} & \cdots & \mu_{2N} \\ \mu_{31} & \mu_{32} & \sigma_3^2 & \cdots & \mu_{3N} \\ \vdots & \vdots & \vdots & \ddots & \vdots \\ \mu_{N1} & \mu_{N2} & \mu_{N3} & \cdots & \sigma_N^2 \end{bmatrix},$$

$$\mu_{ij} = \mu_{ji} = \rho_{ij}\sigma_{i1}\sigma_{j1}, \qquad i, j = 1, \cdots, N \text{ , and } i \neq j.$$

The cross correlation coefficient between the interfering signals from the *ith* and *jth* base stations can be simply approximated as [37]

$$\rho_{ij} = 0.9 - \frac{|\theta|}{200}, \tag{4.22}$$

where θ is the angular degree between the "rays" from the mobile station to the two base stations. The performance of one such system is shown in Fig. 4.4. The physical location of the user is still (0.5, 0.5). Although the numerical value obtained for the BER is very similar to the Viterbi's model, they are two different ways to characterize the log-normal shadowing effect.

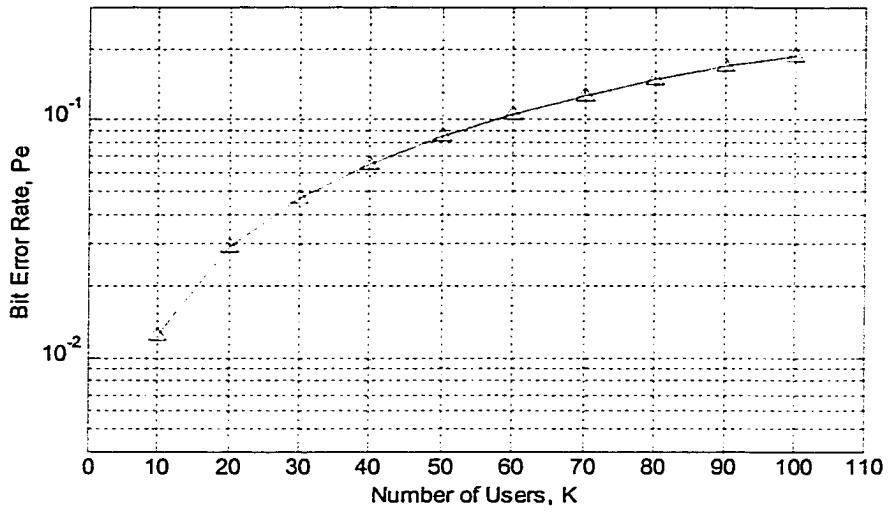


Fig. 4.4. Performance of 7-cell configuration incorporating Mawira's model at location (0.5, 0.5) for the forward link with different number of users.

4.5 Sectorized Antennas in a Multicell Environment

In practical CDMA systems, sectorized antennas are used at each base station for further capacity enhancement. Perfect sectorization of each cell can improve system capacity by three times. However, practical antennas are not perfect and usually they cannot improve the capacity as much as three times. A finite front-to-back ratio is one of the reasons for the performance degradation. In this section, the performance of imperfect sectorization with finite front-to-back ratio for a multicell environment is investigated. Fig. 4.5 shows all the sectors in the 7-cell environment that point directly at the tagged mobile at the central cell

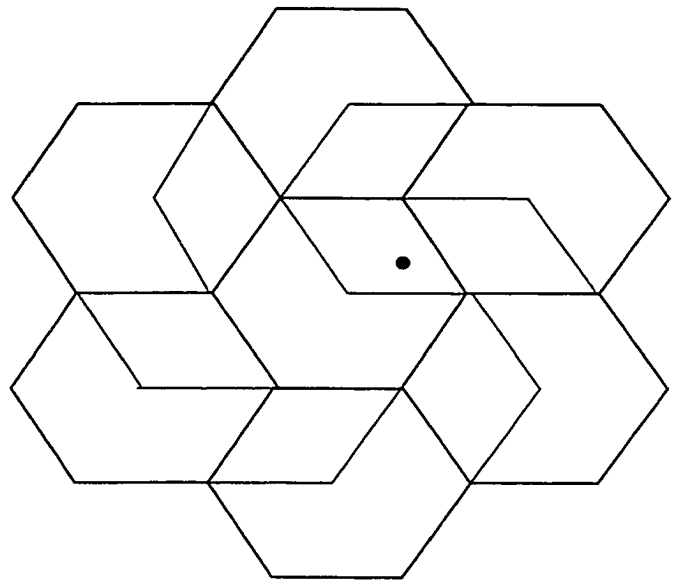


Fig. 4.5. Interfering sectors in a sectorized multicell environment.

which is represented as a dot in the figure. If we consider the effect of finite front-to-back ratio, then besides the interference coming from the sectors which are pointing directly at the tagged mobile, there is other partial interferences which depend on the finite front-to-back ratio and come from the other sectors that are not pointing directly at the tagged mobile. If we denote the front-to-back ratio as Δ, then the BER expression considering the imperfect sectorization can be easily derived as [39]:

$$P_e(x,y) = \int_0^{\infty} dW \int_{-\infty}^{+\infty} d\delta_{1,1} \cdots \int_{-\infty}^{+\infty} d\delta_{N,1} \; pdf_W(W) pdf_{\delta_{1,1},\cdots,\delta_{N,1}}(\delta_{1,1},\cdots,\delta_{N,1}) \cdot Q\left(\left[\frac{((K-1)+KW)\cdot(1+2\Delta)}{3M}\right]^{-1/2}\right). \tag{4.23}$$

The numerical evaluation results of the systems incorporating pure fading, Viterbi's and Mawira's shadowing models are shown in Figs. 4.6, 4.7 and 4.8,

respectively. We can see from these figures, that when the front-to-back ratio increases from 0 dB to 30 dB, the performance of the system improves. For a practical front-to-back ratio of 20 dB, the performance is already very close to the ideal situation.

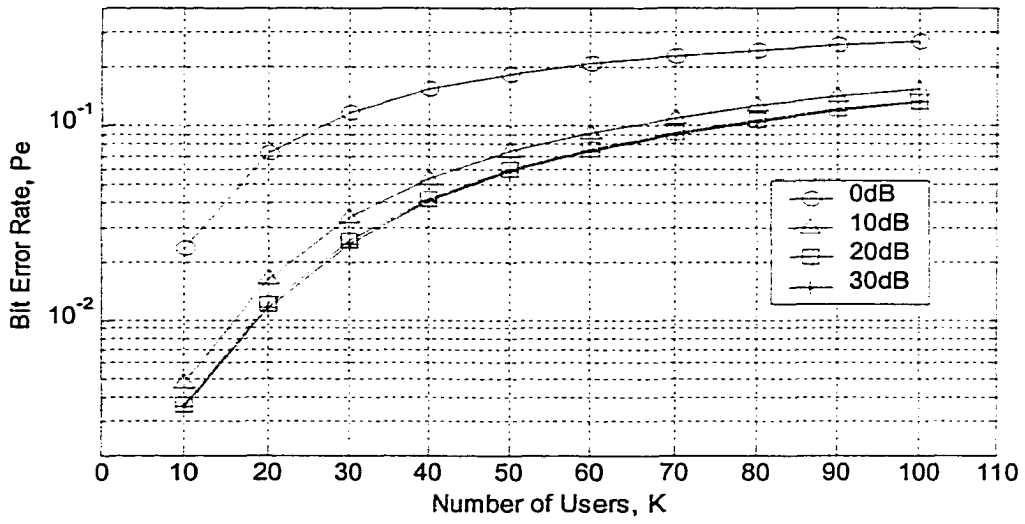


Fig. 4.6. Performance of sectorization and pure fading with finite front-to-back ratios.

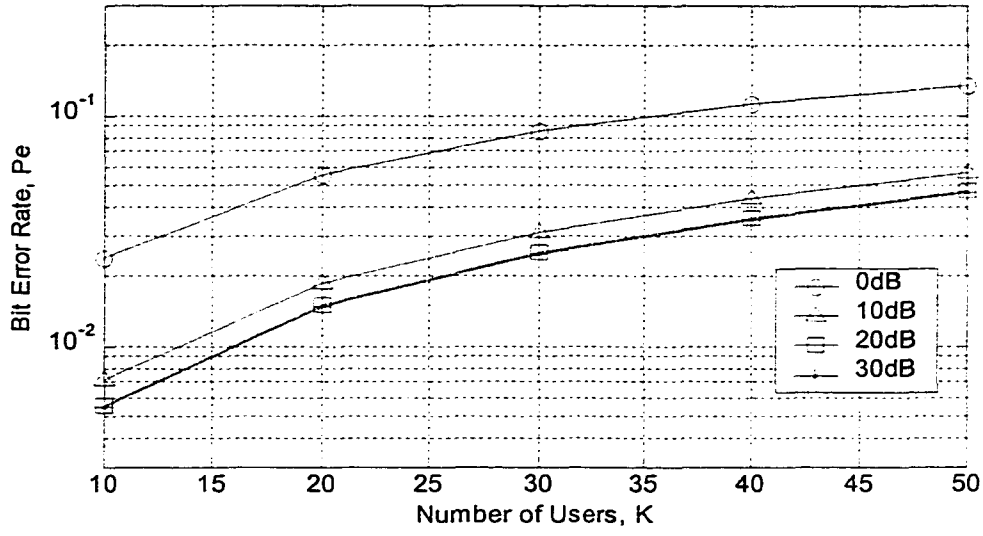


Fig. 4.7. Performance of sectorization of a system incorporating Viterbi's shadowing model with finite front-to-back ratios and $b^2 = 0.5$.

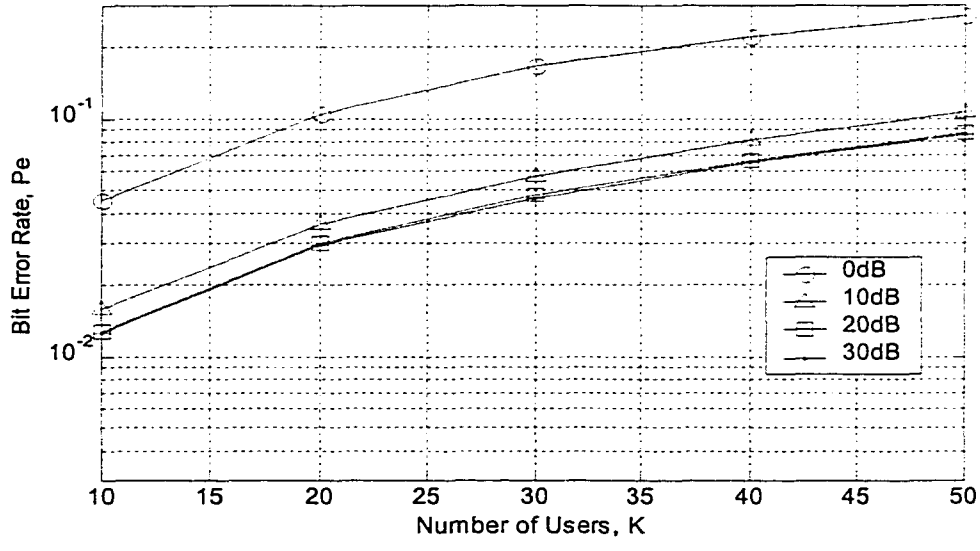


Fig. 4.8. Performance of sectorization of a system incorporating Mawira's shadowing model with finite front-to-back ratios.

4.6 Conclusions

This chapter describes an analytical method to compute the BER of a user with a random location in a CDMA system for a multicell environment. Based on the idea of the combined PDF method introduced by Cheah [34], we considered three phenomena which exist in the field and directly influence the performance of CDMA systems: path loss, log-normal shadowing and Rayleigh fading. The number of integrals for the BER expression is greatly reduced using the extended combined PDF method. For the situation of pure fading, the number of integrals in the simplified expression is not influenced by the number of interfering cells. We can see from our numerical results that there is a small difference in BER between a 19-cell and a 7-cell configuration. However, the number of integrals increases with the number of interfering cells after we include log-normal shadowing effects in our analysis. We considered two shadowing models in this chapter. From the numerical results of a 7-cell configuration incorporating Viterbi's shadowing model, we can see that the BER performance improves when the common part belonging to the mobile user increases. Also we derived the BER expression including the crosscorrelation for all the "rays" coming to the mobile user from the base stations in both the central and interfering cells based on Mawira's correlated log-normal shadowing model. Numerical results for the performance of a 7-cell configuration incorporating his simple approximation formula for the crosscorrelation coefficient between signals and interferences are provided in this chapter. Perfect sectorization can triple the capacity of the

system in a multicell environment. We found from our numerical results on imperfect sectorization that practical front-to-back ratios of 20 dB will not influence the capacity of the system very much.

We use Gauss's formula to perform the numerical integration. It is well known that the truncation error and computation time increase with larger number of integration folds. We have reduced their number by half by using the combined PDF method.

Chapter 5

Conclusions

Performance enhancement techniques such as digital beamforming and coding schemes will play a very important role in future CDMA systems. Adaptive beamforming can steer the beam towards the desired mobile station and place nulls at the interferers. If the number of interferers are less than the number of antenna elements, then the adaptive beamforming performs best. But if there are many more interferers than the number of antenna elements, which is usually the case in a practical situation, then adaptive beamforming cannot track all the interferers and the system performance will not be improved. Furthermore, for the case of reference based adaptive beamforming, the performance is heavily dependent on the reliability of the reference signal. Erroneous reference signals will result in performance degradation instead of enhancement. On the other hand, fixed multibeam techniques seem to be more robust. Their contribution to performance improvement will not be decreased with either increasing number of users or increasing speeds of users. And what is more important is that fixed multibeam techniques can be implemented more easily in the practical world. Compared with adaptive beamforming, switching fixed multibeam techniques may be a better choice for CDMA systems.

Coding techniques are another way to improve the capacity of CDMA systems. They use redundancy bits to increase the error-correcting capability of the system. Investigation of the performance of convolutional, turbo and LDPC coding for IS-2000 systems showed that for the lower data rates, when the corresponding codeword sizes are not large enough, neither turbo nor LDPC coding can achieve the performance of convolutional coding. But when the data rates are higher, which corresponds to longer codewords, both turbo and LDPC coding outperform convolutional coding just as they do for AWGN channels. However, turbo coding performs even better than the randomly generated LDPC codes. Compared with turbo decoding, LDPC coding requires much less decoding complexity, although it has larger memory requirements.

The capacity of CDMA systems is multiple access interference limited. The performance of antenna and coding techniques were investigated using link level simulation of CDMA systems, because it is more realistic and includes all the necessary components which are important in the performance evaluation of the system. However, the computational work for link level simulation of multicell environments is exorbitant. In the antenna performance evaluation, because we have to capture the angles of arrival of the desired user and interferers, we considered modulation of each respective user and assumed perfect power control for all the interferers. The fading, shadowing and path loss for interferences are ignored and only Rayleigh fast fading and power control for the desired user are included in this situation. In the coding performance evaluation, the mutiple

access interference is simply approximated as a Gaussian process, whose variance is determined by the input value of mobile location geometry. However, the multiple access interference effect is quite complicated in a practical situation. In Chapter 4, we evaluated the BER performance of the user in the central cell with the signal and interferences coming from both the base station in the central cell and the base stations in the surrounding cells respectively. The path loss, correlated log-normal shadowing and Rayleigh fast fading phenomena are considered for both the signal and interferences. With the help of a combined PDF simplification method, the models incorporating Viterbi's and Mawira's correlated shadowing effect for each specific physical location of the user are provided and numerically evaluated. It is found that the larger the correlation between the signals and interferences, the better the performance. Also the imperfect sectorization in a multicell environment is investigated for this situation. The practical 20dB front-to-back ratio will not influence the performance significantly.

References

[1] L. Harte, M. Hoenig, D. McLaughlin and R. K. Kta, *"CDMA IS-95 for Cellular and PCS,"* New York: McGraw-Hill Telecommunications, 1999.

[2] S. G. Glisic and P. A. Leppanen, *"Code Division Multiple Access Communications,"* Netherlands: Kluwer Academic Publishers, 1995.

[3] *"Mobile Station-Base Station Compatibility Standard for Dual-Mode Wideband Spread Spectrum Cellular System"*, TIA/EIA/IS-95-A, May 1995.

[4] *"Physical Layer Standard for cdma2000 Spread Spectrum Systems"*, TIA/EIA/IS-2000.2 (Ballot Version), 1999.

[5] F. Adachi, M. Sawahashi and H. Suda, "Wideband DS-CDMA for Next-Generation Mobile Communications Systems," *IEEE Commun. Magazine*, vol. 36, pp. 56-69, Sep. 1998.

[6] J. H. Winters, "Smart antennas for wireless systems," *IEEE Person. Commun.*, pp. 23-27, vol. 5, Feb. 1998.

[7] W. C. Jakes, Jr. *et al.*, *"Microwave Mobile Communications,"* New York: Wiley, 1974.

[8] P. Rooyen, M. Lotter and D. Wyk, *"Space-time Processing for CDMA Mobile Communications,"* Massachusetts: Kluwer Academic Publishers, 2000.

[9] J. Litva and T. K. Lo, *"Digital Beamforming in Wireless Communications,"* Norwood: Artech House, 1996.

[10] S. Lin and D. J. Costello, Jr., *Error Control Coding: Fundamentals and Applications*, Prentice Hall, Englewood Cliffs, New Jersey, 1983.

[11] R. G. Gallager, "Low-density parity-check codes," *IRE Trans. Inform. Theory*, vol. IT-8, pp. 21-28, Jan. 1962.

[12] D. J. C. MacKay, "Good error-correcting codes based on very sparse matrices," *IEEE Trans. Inform. Theory*, vol. 45, pp. 399-431, March 1999.

[13] P. Dent, G. E. Bottomley and T. Croft, "Jake's fading model revisited," *Electron. Letters*, vol. 29, pp.1162-1163, June 1993.

[14] H. J. Xing, J. R. Cruz and Y. Wang, "Fixed multibeam antennas versus adaptive arrays for CDMA systems," in *Proc. IEEE 50th Veh. Technol. Conf.*, pp. 27-31, 1999.

[15] L. M. A. Jalloul and J. M. Holtzman, "Performance analysis of DS/CDMA with noncoherent M-ary orthogonal modulation in multipath fading channels," *IEEE J. of Select. Areas Commun.*, vol. 12, pp. 862-870, June 1994.

[16] A. Sampath, P. S. Kumar and J. M. Holtzman, " On setting reverse link target SIR in a CDMA system," in *Proc. IEEE 47th Veh. Technol. Conf.*, pp. 929-933, 1997.

[17] Y. J. Liu, " Soft decision decoding of a bit-interleaved convolutionally encoded code division multiple access system over Rayleigh fading channels," in *Proc. IEEE 3rd Internat. Symp. Personal Indoor and Mobile Radio Commun.*, 1992, pp. 128-132.

[18] R. A. Monzingo, and T.W.Miller, "*Introduction to Adaptive Arrays,*" New York: John Wiley & Sons, 1980.

[19] C. A. Balanis, *"Antenna Theory: Analysis and Design,"* New York: Harper & Row, 1982, ch. 6, pp. 217-221.

[20] E. Tiedemann, T. Chen, and J. Odenwalder, " Reverse link simulation results," QUALCOMM Incorporated, January 9, 1995

[21] D. J. C. MacKay and R. M. Neal, "Near Shannon limit performance of low density parity check codes," *Elect. Lett*, vol. 33, pp. 457, 1997.

[22] H. J. Xing, R. M. Todd, J. R. Cruz, and Y. Wang, "Comparison of low-density parity-check codes and turbo codes for 3G CDMA systems," submitted to *IEEE Commun. Lett., 2001*

[23] S. Lundby and T. Chen, "Forward link closed loop power control method for cdma2000," Qualcomm Incorporated, 1998.

[24] D. J. C. MacKay, S.T. Wilson and M.C. Davey, "Comparison of constructions of irregular Gallager codes", in *Proc. Annual Allerton Conf. Commun. Control and Computing,* 1998, pp. 220-229.

[25] H. Song, R.M. Todd, and J.R. Cruz, "Low-density parity check codes for magnetic recording channels," *IEEE Trans. Magn.*, vol. 36, September 2000.

[26] J. L. Fan, "Constrained coding and soft iterative decoding for storage," Ph. D. Dissertation, Stanford University, December 1999.

[27] A. J. Viterbi, "An intuitive justification and a simplified implementation of the MAP decoder for convolutional codes," *IEEE J. Select. Areas Comm.*, vol. 16, pp. 260-275, February 1998.

[28] P. Frenger, "Multirate codes and multicarrier modulation for future communication systems," Ph. D. Dissertation, Chalmers University of Technology, Goteborg, 1999.

[29] M. Abdel-Hafez and M. Safak, "Performance analysis of digital cellular radio systems in Nakagami fading and correlated shadowing environment," *IEEE Trans. Veh. Technol.*,vol. 48, pp. 1381-1391, Sep. 2000.

[30] K. S. Butterworth, "Influence of correlated shadowing on the system capacity of a DS-CDMA in-building wireless communication system, " *Wireless Personal Communications: Improving Capacity, Services, and Reliability*, edited by T. S. Rappaport, *et al.*, Massachusetts: Kluwer Academic Publishers, pp. 25-36, 1997.

[31] T. Eng and L. B. Milstein, "Coherent DS-CDMA performance in Nakagami multipath fading," *IEEE Trans. Commun.*, vol. 43, pp. 1134-1143, Feb. 1995.

[32] G. P. Efthymoglou, V. A. Aalo and H. Helmken, "Performance analysis of coherent DS-CDMA systems in a Nakagami fading channel with arbitrary parameters," *IEEE Trans.Veh. Technol.*,vol. 46, pp. 289-297, May 1997.

[33] V. Aalo, O. Ugweje and R. Sudhakar, "Performance analysis of a DS/CDMA system with noncoherent M-ary orthogonal modulation in Nakagami fading," *IEEE Trans. Veh. Technol.*,vol. 47, pp. 20-29, Feb. 1998.

[34] K. L. Cheah, S. W. Oh, and K. H. Li, "Efficient performance analysis of asynchronous cellular CDMA over Rayleigh-fading channels," *IEEE Commun. Letters*, vol. 1, pp. 71-73, May 1997.

[35] S. W. Oh, K. L. Cheah and K. H. Li, "Forward-link BER analysis of asynchronous cellular DS-CDMA over Nakagami-faded channels using combined PDF approach," *IEEE Trans. Veh. Technol.*, vol. 49, pp. 173-180, Jan. 2000.

[36] A. J. Viterbi, "*CDMA: Principles of Spread Spectrum Communication*," Massachusetts: Addison-Wesley Wireless Communications Series, pp. 185-187, 1995.

[37] A. Mawira, "Models for the spatial correlation functions of the (Log)-Normal component of the variabilility of VHF\UHF field strength in urban environment," *IEEE 3rd Inter. Symp. Personal Indoor and Mobile Radio Commun.*, pp. 436-440, 1992.

[38] R. J. Larsen and M. L. Marx, *"An Introduction to Mathematical Statistics and Its Applications,"* New Jersey: Prentice-Hall, 1986.

[39] A. Sathyendran, K. W. Sowerby and M. Shafi, "A statistical approach to the analysis of DS/CDMA cellular systems employing RAKE receivers and sectorized antennas," *IEEE Trans. Veh. Technol.*, vol. 48, pp. 8-19, Jan. 1999.

[40] K. S. Shanmugan and A.M. Breipohl, *"Random Signals: Detection, Estimation and Data Analysis,"* New York: John Wiley & Sons, Inc, 1988.